Geol. Mag.: page 1 of 19. © 2008 Cambridge University Press
doi:10.1017/S0016756808004949

Time-evolution of magma sources in a continental back-arc setting: the Cenozoic basalts from Sierra de San Bernardo (Patagonia, Chubut, Argentina)

SANDRO BRUNI*†, MASSIMO D'ORAZIO*†‡, MIGUEL J. HALLER§, FABRIZIO INNOCENTI*†, PIERO MANETTI¶†, ZOLTÁN PÉCSKAY# & SONIA TONARINI†

*Dipartimento di Scienze della Terra, Università di Pisa, Via S. Maria 53, I-56126 Pisa, Italy
†Istituto di Geoscienze e Georisorse, C.N.R., Via Moruzzi 1, I-56124 Pisa, Italy
§Universidad Nacional de la Patagonia San Juan Bosco, CENPAT-CONICET, Puerto Madryn, Argentina
¶Dipartimento di Scienze della Terra, Università degli Studi di Firenze, Via La Pira 4, I-50121 Florence, Italy
#Institute of Nuclear Research, Hungarian Academy of Sciences, H-4026 Debrecen, Hungary

(*Received* 19 June 2007; *accepted* 2 October 2007)

Abstract – East of the Patagonian Andes, mafic volcanic rocks (mainly lava flows and scoriae) are exposed in the Sierra de San Bernardo fold belt and neighbouring areas (central Patagonia; 44.5–46° S, 69–71° W). They were erupted over a wide interval of time (late Eocene–Pleistocene; 14 new K–Ar ages), and show systematic chemical and Sr–Nd–Pb isotopic variations in time. The alkaline lavas (Mg number 57–66) erupted during the late Eocene and early Miocene, have an intraplate geochemical affinity, and have the highest $^{143}Nd/^{144}Nd$ and $^{206}Pb/^{204}Pb$ and the lowest $^{87}Sr/^{86}Sr$ ratios of the dataset. Their compositions indicate that their depth of equilibration in the mantle was greater than that of subsequent lavas. In contrast, the Plio-Pleistocene alkaline lavas (Mg number 58–71) are the most enriched in incompatible elements, still showing an intra-plate signature, and have the lowest $^{143}Nd/^{144}Nd$ and $^{206}Pb/^{204}Pb$ and the highest $^{87}Sr/^{86}Sr$ ratios. A distinctive group of early Miocene subalkaline lavas is characterized by slightly more evolved compositions (Mg number 56–59), coupled with very low incompatible element contents, flat LREE and fractionated HREE patterns ('kinked' pattern), and intermediate Sr–Nd–Pb isotope compositions. The Pleistocene basanites (Mg number 71–72) from the Cerro Ante monogenetic cone, on the easternmost slopes of the Patagonian Andes, have a marked orogenic geochemical signature and Sr–Nd–Pb isotope ratios that overlap with those of volcanic rocks from the adjacent active Andean arc. They originated in a mantle source extensively modified by the addition of materials from the subducting Pacific oceanic plates. We suggest that the wide chemical and isotopic variability of the Sierra de San Bernardo lavas reflects the upwelling of asthenospheric mantle beneath the study area, which induced lithospheric erosion and progressive involvement of enriched mantle domains in the genesis of magmas. In this context, late Eocene and early Miocene alkaline magmatism was dominantly sourced from the asthenospheric mantle, whereas Plio-Pleistocene alkaline magmas contain the largest proportion of an enriched lithospheric component. The peculiar compositional features of the early Miocene subalkaline lavas are interpreted in terms of high-degree mantle melting followed by melt–lithospheric mantle reaction processes. Based on current knowledge about the relative movement and decoupling between lithosphere and asthenosphere, we propose that the asthenosphere below the study area rose up to compensate for the westward drift of the mantle wedge coupled with the South American lithosphere.

Keywords: Patagonia, basaltic rocks, Cenozoic, petrogenesis, geodynamics, isotope geochemistry.

1. Introduction

Understanding the origin and geodynamic significance of continental mafic magmas and the composition of their sources is one of the main goals of igneous petrology. In back-arc continental settings, the complex nature of subduction-related processes and the high number of geochemical reservoirs potentially involved in magma genesis and evolution make it difficult to meet these goals. Magmas erupted in continental back-arc regions may contain inputs from the sub- and supra-slab asthenosphere, the subducted oceanic lithosphere (melts/fluids from subducted igneous and sedimentary rocks), the subcontinental lithospheric mantle and the lower and upper continental crust. Over the last three decades, many studies have focused on one of the most important occurrences of mafic magmatism in continental back-arc settings, namely, the Cenozoic Patagonian Basaltic Province (e.g. Baker *et al.* 1981; Stern *et al.* 1990; Ramos & Kay, 1992; Gorring *et al.* 1997; D'Orazio *et al.* 2004; Fig. 1). Throughout the Cenozoic, large volumes of alkaline and subalkaline basaltic lavas and subordinate amounts of more differentiated products erupted in extra-Andean Patagonia (Argentina and Chile), behind the Andean volcanic arc. Most published studies focus on the southernmost occurrences of this magmatism and emphasize the dominant role played in the

‡Author for correspondence: dorazio@dst.unipi.it

petrogenesis of these basalts by ridge–trench collision and slab window opening under this sector of Patagonia (e.g. Ramos & Kay, 1992; Gorring *et al.* 1997; D'Orazio *et al.* 2000, 2001, 2005; Gorring & Kay, 2001; Gorring *et al.* 2003; Espinoza *et al.* 2005). More recently, mafic magmatic rocks from northern Patagonia (Meseta de Somuncura: de Ignacio *et al.* 2001; Kay *et al.* 2007; Crater Basalt Volcanic Field: Massaferro *et al.* 2006; Neuquén Basin: Kay & Copeland, 2006) have been investigated, and several hypotheses alternative to slab window opening have been proposed for their genesis.

In this paper we report on the geochronology, petrography, geochemistry and Sr–Nd–Pb isotope composition of basaltic rocks exposed in a wide area of central Patagonia between the Patagonian Andes and Musters Lake (Chubut Province, Argentina; Fig. 1). The volcanic rocks found in this area were erupted over a time interval of about 35 Ma (from the late Eocene to the Pleistocene) and show wide chemical and isotopic variability. In addition, they were erupted just north of the vertical projection of the Neogene slab window thought to occur beneath southern Patagonia. Accordingly, the study of these rocks provides a good opportunity to better characterize the nature of Cenozoic basaltic magmatism in Patagonia and to test geodynamic models, alternative to the slab window model, for the genesis of basaltic magmas in the back-arc region of the Patagonian Andes.

2. Geological outline and geochronology

The study area (44.5–46° S, 69–71° W) is located in the back-arc region of the Patagonian Andes, in the central-western sector of the Golfo San Jorge Basin (Fig. 1). The latter is a dominantly extensional Mesozoic basin which trends east–west from the Andes to the Atlantic Ocean and is bounded to the north and south by the North Patagonian and Deseado massifs, respectively (Fitzgerald *et al.* 1990; Sylwan, 2001). These massifs represent part of a late Proterozoic–middle Palaeozoic orogenic belt that extended along the southwestern margin of Gondwana (Pankhurst *et al.* 2006). At the latitude of the study area the Andes comprise, from west to east, the following main structural units: (1) a deformed Palaeozoic metamorphic basement (Coastal Cordillera) exposed in the Chonos Archipelago and in the Taitao Peninsula (Hervé *et al.* 1981); (2) an active Quaternary volcanic arc, in part related to the activity of the dextral strike-slip Liquiñe–Ofqui fault system (Cembrano, Hervé & Lavenu, 1996); (3) the Jurassic to Miocene calc-alkaline Patagonian Batholith and the Andean front.

A large portion of the study area is occupied by the Sierra de San Bernardo, a thick-skinned fold belt running approximately N–S (Fig. 2). The Sierra de San Bernardo predominantly consists of continental Cretaceous sedimentary rocks (Chubut Group; Fitzgerald *et al.* 1990; Sylwan, 2001; Hechem & Strelkov, 2002) and by Cenozoic (Priabonian to Pleistocene) igneous

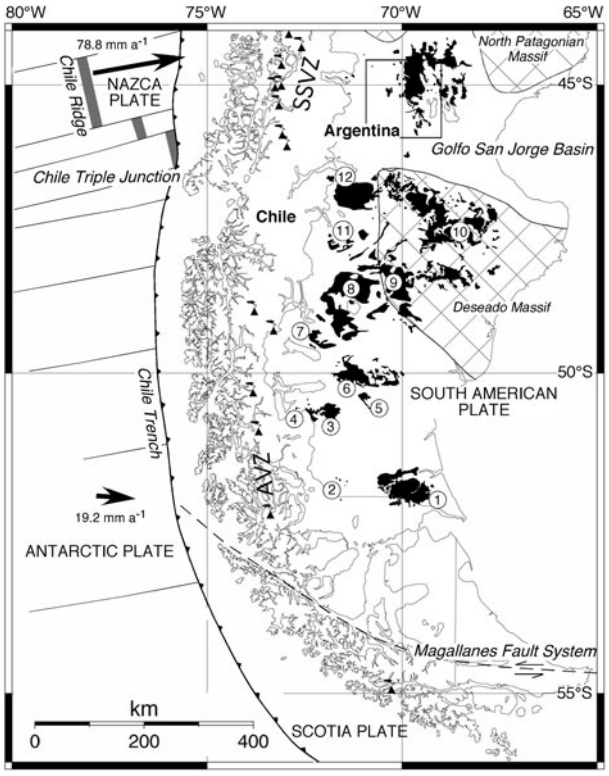

Figure 1. Schematic geodynamic setting of southern South America and the adjacent Pacific Ocean. The sketch shows: the fracture zones of the oceanic Nazca and Antarctic plates (thin continuous lines), the Chile oceanic spreading ridge (grey strips), the Chile trench (heavy continuous line with triangles on the overriding plate), the transcurrent margin between the Scotia and South American plates (dashed line), the Chile Triple Junction, the main active volcanoes of the Southern South Volcanic Zone (SSVZ) and Austral Volcanic Zone (AVZ) of the Andes (black smoking triangles), the Cenozoic Patagonian lavas (black areas). The two large, black arrows are the convergence vectors of the Nazca and Antarctic plates with respect to South America according to the HS3-NUVEL-1A model (Gripp & Gordon, 2002). Circled numbers indicate the main Patagonian basalt occurrences cited in the text: 1 – Pali Aike Volcanic Field (late Pliocene–Quaternary); 2 – Estancia Glencross area (late Miocene); 3 – Meseta de las Vizcachas (middle Miocene–late Pliocene); 4 – C. del Fraile (late Pliocene–Quaternary); 5 – Camusú Aike Volcanic Field (late Pliocene); 6 – Mesetas on the north side of the Río Santa Cruz valley (Laguna Amenida–Condor Cliff area; Miocene?–late Pliocene); 7 – Meseta del Viento (early Pliocene–late Pliocene); 8 – Meseta de la Muerte and Meseta Strobel (middle Miocene–early Pliocene); 9 – Meseta Central (late Miocene–late Pliocene); 10 – Mesetas of the Northeast region (Eocene–late Pliocene); 11 – Meseta Belgrano (late Miocene–late Pliocene); 12 – Meseta del Lago Buenos Aires and Meseta Chile Chico (Paleocene–Quaternary). The rectangle encloses the study area.

mafic rocks. During Tertiary times (probably Miocene: Chelotti, 1997), these rocks were deformed and uplifted by compressional stresses that caused the tectonic inversion and reactivation of pre-existing Mesozoic normal faults (Homovc *et al.* 1995). The volcanic rocks of the Sierra de San Bernardo mainly occur as sequences of mafic lavas, sometimes forming plateaux, erupted from small and variably eroded volcanic cones.

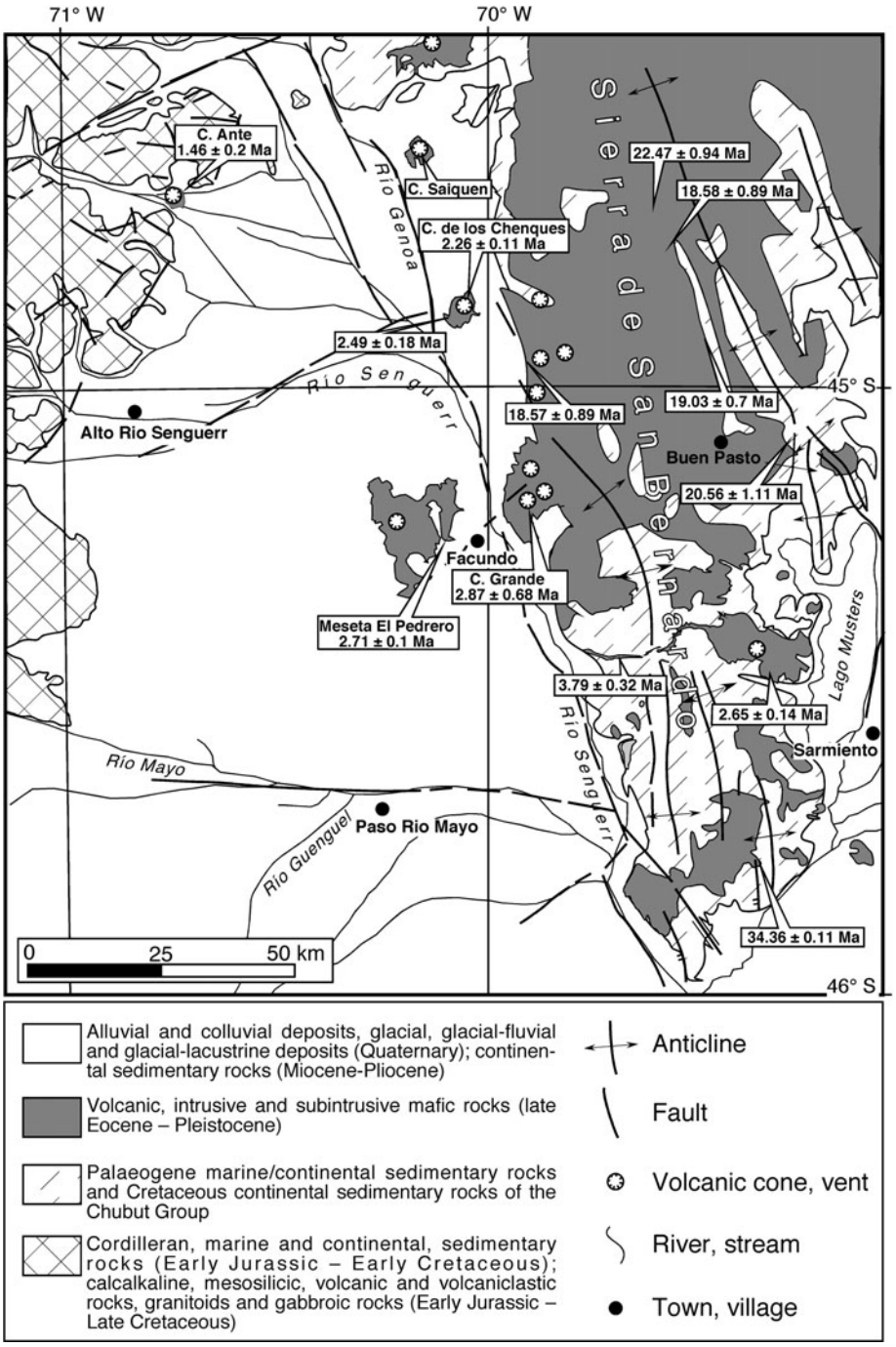

Figure 2. Geological sketch map of the study area, redrawn and largely simplified from Lizuain, Ragona & Folguera (1995).

The lava flow sequences and sedimentary rocks are locally intruded by small stocks, sills, necks and dykes of olivine gabbro and microgabbro. The west side of the Sierra de San Bernardo abruptly ends in a wide plain which is crossed by the rivers Senguerr and Genoa. The boundary between Sierra de San Bernardo and the plain is marked by several well-preserved scoria cones aligned along a NNW–SSE trend (Fig. 2). These features are indicative of the possible extensional nature of the Genoa–Senguerr valley.

Fourteen new K–Ar age determinations were made on lavas from the study area (Table 1). These ages significantly enlarge the existing dataset (Baker *et al.* 1981; Marshall *et al.* 1986), allowing the identification of three phases of volcanic activity separated by relatively long (10 and 15 Ma) intervals of time (Fig. 3): (1) late Eocene (Priabonian, *c.* 35 Ma); (2) late Oligocene–early Miocene (Chattian–Burdigalian, 25–18 Ma); (3) Plio-Pleistocene (Zanclean–Early Pleistocene, 3.8–1.5 Ma). A sample of a lava flow from the Cerro Grande scoria cone (PA-403; Fig. 2) was found to contain radiogenic ^{40}Ar below the detection limit of the adopted method (Table 1). This may indicate the occurrence of volcanic activity younger than Early Pleistocene, as also suggested by the well-preserved morphology of the exposed surface of this flow.

Table 1 K–Ar data

Sample	K (wt %)	^{40}Ar rad ($\times 10^{-7}$ cm^3 STP/g)	^{40}Ar rad (mol. %)	Age (Ma) $\pm 1\sigma$	Epoch	Stage
PA 425	0.85	11.45	66.0	34.36 ± 1.11	Eocene	Priabonian
PA 417	1.43	12.58	38.3	22.47 ± 0.94	Miocene	Aquitanian
PA 394	0.73	5.884	27.1	20.56 ± 1.11	Miocene	Aquitanian
PA 397	0.61	4.515	47.7	19.03 ± 0.70	Miocene	Burdigalian
PA 414	0.99	7.158	31.3	18.58 ± 0.89	Miocene	Burdigalian
PA 419	0.42	3.026	31.1	18.57 ± 0.89	Miocene	Burdigalian
PA 382	1.67	2.463	16.2	3.79 ± 0.32	Pliocene	Zanclean
PA 400	2.44	2.739	5.6	2.87 ± 0.68	Pliocene	Piacenzian
PA 421	2.21	2.328	47.2	2.71 ± 0.10	Pliocene	Piacenzian
PA 380	1.48	1.528	27.6	2.65 ± 0.14	Pliocene	Piacenzian
PA 409	2.42	2.346	19.4	2.49 ± 0.18	Pliocene	Gelasian
PA 406	2.25	1.976	30.7	2.26 ± 0.11	Pliocene	Gelasian
PA 390	3.54	2.016	9.5	1.46 ± 0.20	Pleistocene	
PA 403	1.56	< d.l.	–	–		

< d.l. – below detection limit.

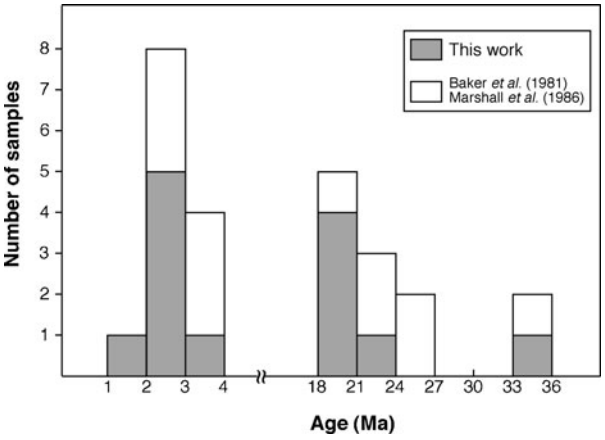

Figure 3. Distribution of new and literature K–Ar ages for mafic lavas from the study area.

The Plio-Pleistocene lavas occurring at the top of Sierra de San Bernardo are undeformed and lie unconformably above the underlying formations (both sedimentary and igneous), whereas the older lavas are sometimes tilted and gently folded, indicating that they underwent the deformation processes responsible for the origin of the Sierra de San Bernardo fold belt. The scoria cones occurring along the eastern side of the Genoa–Senguerr valley, just above the westernmost formations of the Sierra de San Bernardo, formed during the Plio-Pleistocene. A ~ 150 km^2 wide lava field (Meseta El Pedrero, 2.71 Ma) occurs in the central part of the valley (Quartino, 1958; Fig. 2), whereas scattered cones such as Cerro Ante (1.46 Ma; sampled for this study) and Cerro Gato (3.6 Ma; studied by Baker *et al.* 1981) are located on the western side of the Genoa–Senguerr valley, above the easternmost slopes of the Patagonian Andes.

3. Petrography and classification

Volcanic rock samples represent lava flows and subordinate scoriae; they are fresh and only sporadically contain iddingsitic material partially replacing olivine. More weathered rocks containing secondary carbonates and zeolites were found in several localities of Sierra de San Bernardo and were discarded for this study. The studied samples are characterized by subaphyric to moderately porphyritic textures (porphyritic index = 5–20 vol. %) with small, sparsely distributed olivine (5–20 vol. %) and rare clinopyroxene (0–2 vol. %) phenocrysts set in a fine-grained to glassy groundmass. Olivine phenocrysts range from 0.5 to 1 mm in size, show euhedral shapes and, rarely, skeletal structures. Clinopyroxene phenocrysts generally occur in glomerophyric aggregates; they are euhedral, larger (1–2 mm) than olivine and light purple-brown coloured. The crystallinity of the groundmass is variable, ranging from glassy to holocrystalline. It consists of plagioclase, clinopyroxene ± olivine ± Fe–Ti oxides ± alkali feldspar ± glass.

Mantle xenoliths and xenocrysts are very commonly found within the lava flows and the cores of ovoidal and spindle-shaped pyroclastic bombs from the Cerro de los Chenques monogenetic cone (Fig. 2). Xenoliths may reach up to a decimetre in size; they are extremely fresh and are characterized by coarse- to medium-grained protogranular and/or tabular textures. Spinel-bearing dunite, lherzolite, harzburgite, websterite and composite websterite + lherzolite/harzburgite are the dominant lithologies (Rivalenti *et al.* 2004, 2007).

Following the total alkali v. silica classification diagram (Fig. 4), the volcanic rocks from the study area are basanites, trachybasalts, alkaline and subalkaline basalts and basaltic andesites. Based on their degree of alkalinity, K_2O/Na_2O ratios and age, the studied Sierra de San Bernardo volcanic rocks were subdivided as follows: group Ia (basanites, alkali basalts, trachybasalts) includes late Eocene to early Miocene alkaline lavas; group Is (subalkaline basalts, basaltic andesites) includes early Miocene subalkaline lavas; group IINa (alkali basalts, trachybasalts) includes Plio-Pleistocene alkaline lavas with $K_2O/Na_2O < 0.5$; group IIK (basanites, trachybasalts) includes Plio-Pleistocene alkaline lavas with $K_2O/Na_2O > 0.6$. The Pleistocene basanites from Cerro Ante, by virtue of their peculiar chemistry (see Section 4), constitute a separate group.

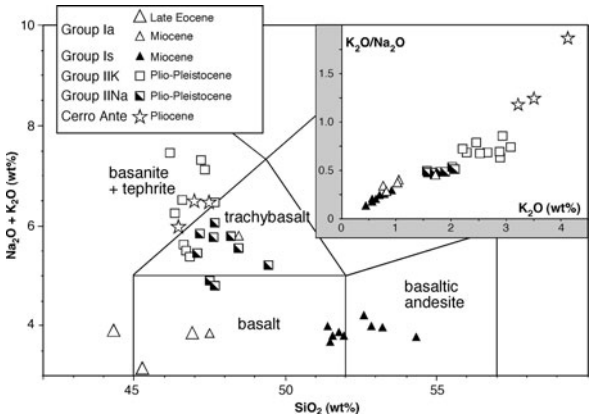

Figure 4. Total alkali v. silica classification diagram for the studied rocks. Inset: K_2O/Na_2O v. K_2O plot.

4. Geochemistry

Major- and trace-element analyses of representative samples from the study area are reported in Table 2. All the alkaline volcanic rocks are near primitive in composition, as indicated by their high Mg numbers (58–72) and high concentrations of MgO (6.8–12.9 wt %), Ni (110–375 ppm) and Cr (90–507 ppm). The basanite lavas from Cerro de los Chenques (samples PA-406–409 and PAT 70) are characterized by high MgO (> 10 wt %) and Ni (> 250 ppm) contents due to contamination by olivine and pyroxene xenocrysts from disaggregated mantle xenoliths (Fig. 5a). The subalkaline volcanic rocks show less primitive compositions, with Mg numbers between 56 and 59 and lower concentrations of MgO (6.1–7.5 wt %), Ni (122–162 ppm) and Cr (238–275 ppm). They show systematically higher Cr/Ni ratios with respect to the alkaline ones, but lower TiO_2 and P_2O_5 contents (Fig. 5b). The basanite lavas from Cerro Ante are characterized by low TiO_2 and $Fe_2O_{3\ tot}$ (Fig. 5b, c) and high CaO contents. The late Eocene lava samples have higher $Fe_2O_{3\ tot}$ contents with respect to the other alkaline lavas with the same Mg numbers (Fig. 5c).

Incompatible element distributions are reported in the primordial mantle-normalized diagrams of Fig. 6. As observed for the majority of Cenozoic alkaline lavas from all of extra-Andean Patagonia (e.g. Stern *et al.* 1990; Ramos & Kay, 1992; Gorring *et al.* 1997; D'Orazio *et al.* 2000, 2004; Guivel *et al.* 2006; Kay *et al.* 2007), alkaline mafic rocks from Sierra de San Bernardo show a within-plate geochemical signature. They show the typical humped distributions, with Nb and Ta peaks and marked negative Pb anomalies (Fig. 6a, b). REE (rare earth elements) distributions (Fig. 7a, b) are remarkably similar: chondrite-normalized REE patterns are almost rectilinear and enriched in LREE (light REE) ($La_N = 91–276$, $Yb_N = 7.9–12.2$, $(La/Yb)_N = 9.7–30.6$). Some samples display a slight positive Eu anomaly.

The most remarkable differences among these alkaline groups are the relative enrichment of the most

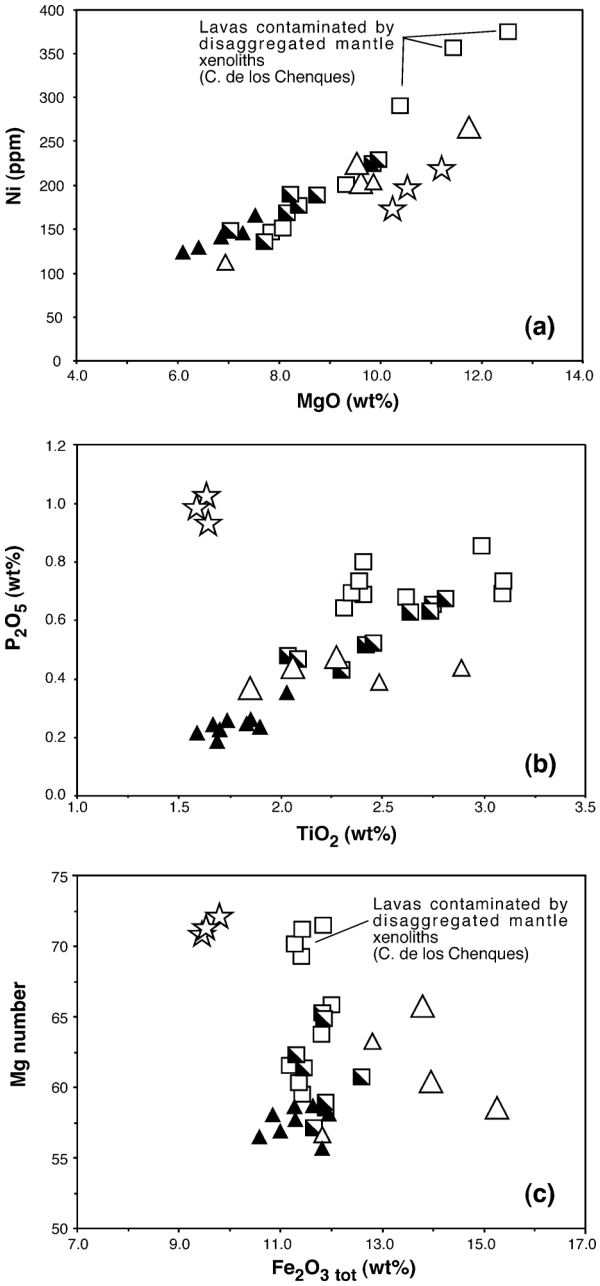

Figure 5. Binary plots illustrating some chemical features of Sierra de San Bernardo and Cerro Ante lavas (symbols as in Fig. 4). (a) Ni (ppm) v. MgO (wt %) plot showing the primitive nature of the studied samples; (b) P_2O_5 (wt %) v. TiO_2 (wt %) plot showing the rough correlation of these elements in Sierra de San Bernardo lavas, and the very high P_2O_5/TiO_2 of basanites from Cerro Ante; (c) Mg number v. $Fe_2O_{3\ tot}$ (wt %) plot showing the high and low total iron contents of group Ia and Cerro Ante lavas, respectively.

incompatible elements and the LREE/HREE (heavy REE) ratios, which increase from group Ia to IINa to IIK, and the systematic occurrence of negative K anomalies in Ia lavas (Fig. 6a).

The subalkaline basalts and basaltic andesites of group Is are characterized by different incompatible element distributions; they are less enriched and less fractionated and show a prominent positive Sr anomaly

Table 2 Whole-rock major and trace element analyses

Sample	PA 424	PA 425	PA 426	PA 414	PA 417	PA 415	PA 419	PA 393	PA 394	PA 397	PA 399	PA 400	PA 402	PA 406	PA 408
Group	Ia	Ia	Ia	Ia	Ia	Is	Is	Is	Is	Is	Is	IIK	IIK	IIK	IIK
Lat. S	44°57.5′	45°44.9′	45°44.6′	44°45.2′	44°33.0′	44°42.3′	45°01.2′	45°07.2′	45°07.1′	45°03.0′	44°55.6′	45°11.9′	45°11.6′	44°52.2′	44°52.2′
Long. W	69°18.2′	69°21.9′	69°24.1′	69°36.0′	69°35.0′	69°36.9′	69°56.6′	69°19.0′	69°20.2′	69°27.7′	69°29.9′	69°58.4′	69°58.1′	70°04.2′	70°04.2′
Classif.	BN	AB	AB	AB	HW	BA	BA	BA	SB	SB	SB	BN	BN	KTB	BN
SiO_2 (wt %)	44.3	47.0	44.4	46.9	47.3	53.4	54.6	52.1	52.1	51.7	49.8	46.8	46.9	46.15	46.0
TiO_2	2.27	1.85	2.01	2.45	2.83	1.59	1.69	1.71	1.70	1.86	1.61	3.06	2.94	2.38	2.59
Al_2O_3	12.9	14.3	13.8	13.6	15.0	15.5	15.3	14.5	14.9	14.8	14.3	14.5	14.4	12.9	13.7
Fe_2O_3	13.8	14.0	15.0	12.6	11.5	11.0	10.6	11.1	11.6	12.0	10.9	11.3	11.0	11.3	11.9
MnO	0.18	0.17	0.18	0.16	0.14	0.15	0.20	0.13	0.14	0.15	0.14	0.14	0.14	0.15	0.15
MgO	11.8	9.55	9.46	9.73	6.79	6.42	6.14	6.74	7.53	7.32	6.84	7.76	7.92	12.4	10.3
CaO	10.4	9.10	9.76	8.93	7.71	8.06	7.90	8.04	8.25	8.45	9.07	7.51	7.84	7.23	7.54
Na_2O	2.84	2.99	2.30	2.75	3.95	3.40	3.35	3.28	3.17	3.23	2.96	4.17	3.42	3.10	3.69
K_2O	1.02	0.82	0.76	1.05	1.72	0.57	0.45	0.64	0.63	0.79	0.70	3.09	2.95	2.48	2.53
P_2O_5	0.46	0.36	0.42	0.44	0.70	0.21	0.18	0.25	0.22	0.25	0.23	0.88	0.83	0.85	0.83
Total	100.0	100.1	98.1	98.6	97.6	100.3	100.4	98.5	100.2	100.6	96.6	99.2	98.3	98.9	99.2
LOI	1.41	0.42	1.17	1.16	1.88	0.30	0.62	0.86	0.78	0.40	2.19	0.55	1.51	1.12	0.71
Mg number	66	61	59	63	57	57	56	58	59	58	59	61	62	71	66
Be (ppm)	1.59	1.24	1.12	1.61	2.72	0.85	0.69	0.87	0.88	0.97		3.13	2.65	2.46	2.71
Sc	25	22	22	19	15	18	20	17	18	20		16	15	16	15
V	250	198	212	189	178	150	156	161	170	182		180	184	149	167
Cr	375	283	229	285	90	238	240	275	274	249		180	195	416	326
Co	62	58	57	52	41	40	45	36	44	46		40	41	47	48
Ni	263	222	199	202	110	125	122	138	162	143		147	152	375	291
Rb	17.2	16.7	16.9	17.2	22.4	9.8	9.8	8.6	12.6	12.9		57	51	45	51
Sr	570	511	542	620	1078	316	284	339	370	394		932	940	820	906
Y	23.3	20.9	22.4	20.0	21.8	19.9	19.7	20.0	18.0	19.7		25.8	24.4	22.6	24.7
Zr	174	125	132	172	347	87	83	91	88	95		379	332	272	301
Nb	50	26.3	32.9	40	73	12.4	8.6	14	14	17.4		74	66	56	62
Cs	0.52	0.45	0.71	0.26	0.64	0.28	0.34	0.19	0.38	0.37		0.96	0.92	0.88	0.95
Ba	280	190	244	324	577	127	159	128	153	190		646	618	499	581
La	31.6	21.5	26.5	24.8	51	9.5	7.0	10.5	9.5	11.8		65	59	50	54
Ce	65	44	55	50	101	19.4	15.3	20.0	21.0	24.2		126	114	97	106
Pr	7.8	5.6	6.7	6.2	11.9	2.6	2.2	2.9	2.8	3.2		14.8	13.5	11.5	12.6
Nd	32.0	23.3	28.0	26.1	47	12.0	11.0	13.8	12.7	14.5		58	53	45	49
Sm	6.4	5.1	6.1	5.8	9.0	3.4	3.6	4.0	3.7	3.9		11.1	10.1	8.3	9.4
Eu	2.27	1.77	2.05	1.79	2.95	1.39	1.35	1.45	1.19	1.60		3.26	2.94	2.79	2.82
Gd	5.0	4.8	5.3	5.2	7.0	3.7	4.2	4.2	3.7	4.0		8.5	8.0	7.0	7.5
Tb	0.84	0.75	0.83	0.74	0.99	0.62	0.67	0.69	0.64	0.67		1.15	1.07	0.92	1.04
Dy	4.5	4.1	4.5	4.0	5.0	3.7	3.8	3.9	3.5	3.8		5.7	5.4	4.8	5.3
Ho	0.81	0.78	0.83	0.72	0.81	0.69	0.69	0.75	0.68	0.70		0.93	0.90	0.82	0.91
Er	2.03	1.83	2.07	1.74	1.78	1.71	1.87	1.72	1.61	1.75		2.10	2.11	1.91	2.04
Tm	0.27	0.24	0.27	0.23	0.23	0.25	0.26	0.23	0.22	0.24		0.27	0.25	0.23	0.26
Yb	1.49	1.51	1.64	1.27	1.29	1.44	1.33	1.35	1.22	1.37		1.45	1.44	1.39	1.48
Lu	0.22	0.22	0.22	0.16	0.17	0.19	0.19	0.18	0.18	0.20		0.17	0.18	0.19	0.20
Hf	3.9	3.06	3.17	4.1	8.0	2.27	2.19	2.30	2.30	2.44		8.3	7.5	5.8	6.8
Ta	2.96	1.57	2.00	2.46	4.8	0.82	0.55	0.91	0.93	1.13		4.7	4.3	3.5	3.9
Pb	2.46	2.25	2.00	1.92	4.2	1.49	1.41	0.93	1.45	1.72		5.6	5.3	4.2	4.7
Th	4.1	2.83	3.17	2.63	6.2	1.27	0.92	1.19	1.40	1.51		7.7	6.7	6.1	6.5
U	1.14	0.75	0.83	0.74	1.71	0.36	0.30	0.37	0.41	0.46		2.04	1.69	1.67	1.76

Table 2. Continued

Sample	PA 409	PA 421	PA 380	PA 382	PA 403	PA 405	PAT 71	PAT 72	PAT182	PAT189	PA 388	PA 389	PA 390	PA 423	PA 391
Group	IIK	IIK	IINa	IINa	IINa	IINa	IINa	IINa	IINa	IINa	C. Ante	C. Ante	C. Ante	Intrusive	Intrusive
Lat. S	44°52.1′	45°17.8′	45°30.4′	45°27.2′	45°12.5′	45°10.2′	44°39.0′	44°39.0′	45°11.0′	45°11.0′	44°42.6′	44°43.0′	44°43.0′	45°41.6′	45°08.8′
Long. W	70°06.5′	70°12.4′	69°20.9′	69°40.3′	70°01.3′	70°00.0′	70°10.5′	70°10.5′	69°58.5′	69°58.5′	70°46.2′	70°46.7′	70°46.7′	69°14.5′	69°12.4′
Classif.	BN	KTB	HW	KTB	KTB	KTB	AB	AB	KTB	KTB	BN	BN	BN	Gabbro	Gabbro
SiO_2 (wt %)	46.3	47.1	46.4	47.7	49.6	48.6	47.3	47.0	46.5	47.9	46.4	46.3	46.8	47.2	49.8
TiO_2	2.38	2.36	2.60	2.81	2.30	2.43	2.02	2.05	2.71	2.43	1.63	1.57	1.62	1.97	2.30
Al_2O_3	13.4	14.8	13.7	15.2	15.1	15.2	14.6	14.6	14.5	14.9	13.9	13.7	13.7	14.9	17.5
Fe_2O_3	11.4	11.9	12.4	11.7	11.3	11.5	11.8	11.7	11.7	11.2	9.79	9.46	9.33	12.7	9.96
MnO	0.15	0.15	0.15	0.14	0.14	0.14	0.16	0.15	0.14	0.14	0.15	0.15	0.14	0.15	0.12
MgO	11.4	9.39	8.61	7.04	8.24	8.18	9.89	9.66	7.57	8.32	11.2	10.4	10.1	7.92	4.52
CaO	7.02	8.92	8.69	8.81	7.98	8.18	8.42	8.33	9.07	8.17	9.87	9.46	9.61	9.54	9.23
Na_2O	3.83	3.26	3.70	4.01	3.55	3.78	3.29	3.17	3.75	3.87	2.73	2.86	2.21	3.42	4.31
K_2O	2.66	2.28	1.69	2.07	1.69	1.80	1.59	1.58	2.01	1.89	3.22	3.51	4.14	1.15	1.55
P_2O_5	0.90	0.64	0.62	0.67	0.44	0.52	0.48	0.46	0.64	0.52	1.03	0.97	0.92	0.32	0.44
Total	99.4	100.8	98.6	100.2	100.3	100.3	99.6	98.7	98.6	99.3	99.9	98.4	98.6	99.3	99.7
LOI	0.88	−0.33	0.24	−0.50	−0.35	0.11	−0.42	0.04	0.22	−0.34	0.06	0.74	0.46	0.25	1.48
Mg number	69	64	61	58	62	62	65	65	59	62	72	71	71	58	51
Be (ppm)	3.03	2.34	2.22	2.32	1.81	2.00	1.72	1.75	2.26	1.94	4.1	3.3	4.4	1.63	1.76
Sc	18	22	19	18	21	17	23	22	17	18	29	31	29	24	21
V	148	229	204	220	196	189	205	207	210	190	258	278	260	217	190
Cr	480	251	233	221	249	223	288	286	241	221	476	500	507	285	127
Co	46	47	47	41	47	43	50	50	44	45	46	42	42	49	30
Ni	355	201	191	148	192	170	230	226	137	178	221	192	174	157	59
Rb	55	59	28.4	35.1	34	32.0	30.6	29.9	29.3	31.8	168	191	219	23.7	25.7
Sr	959	762	836	872	635	721	565	561	839	700	1115	1044	858	434	729
Y	25.0	24.7	24.5	23.6	22.3	22.2	24.4	24.7	23.5	22.5	28.2	26.9	24.8	21.6	22.0
Zr	341	251	233	262	199	218	170	168	251	215	309	314	331	176	175
Nb	70	38	54	56	34	40	32.3	32.1	53	39	17.8	17.0	14.2	37	40
Cs	1.01	1.00	0.61	0.67	0.65	0.56	0.62	0.60	0.30	0.53	5.2	6.2	7.0	0.80	0.35
Ba	565	460	388	428	355	370	334	354	411	375	573	551	477	222	332
La	60	40	42	45	30.4	34	30.0	29.6	44	35	57	52	37	23.8	26.2
Ce	115	86	82	90	61	69	59	57	86	70	130	121	94	49	52
Pr	13.4	10.9	10.0	11.0	7.4	8.3	7.1	7.0	10.6	8.5	17.3	16.4	13.8	6.0	6.5
Nd	52	44	40	44	31.0	34	28.3	28.0	42	34	71	68	59	24.2	27.4
Sm	9.7	8.5	8.1	8.4	6.5	7.2	5.9	5.9	8.2	7.0	11.0	11.3	9.3	5.5	6.1
Eu	3.14	2.31	2.86	2.65	1.93	2.46	1.80	1.84	2.61	2.19	2.89	2.68	2.21	1.89	2.11
Gd	7.6	6.6	6.9	7.1	5.6	5.5	5.3	5.4	7.1	6.1	7.8	7.6	6.4	4.9	5.6
Tb	1.02	0.98	0.99	1.01	0.82	0.86	0.86	0.84	0.96	0.87	1.00	1.02	0.86	0.76	0.85
Dy	5.3	5.1	5.1	5.1	4.4	4.8	4.6	4.7	4.9	4.6	5.1	5.0	4.6	4.4	4.6
Ho	0.90	0.94	0.89	0.86	0.82	0.80	0.88	0.91	0.88	0.83	0.97	0.95	0.88	0.80	0.79
Er	2.04	2.17	2.00	2.00	1.89	1.94	2.22	2.33	1.96	2.00	2.47	2.37	2.25	1.98	2.01
Tm	0.25	0.30	0.25	0.25	0.26	0.22	0.30	0.32	0.24	0.25	0.33	0.35	0.32	0.28	0.24
Yb	1.49	1.73	1.49	1.39	1.44	1.49	1.83	1.94	1.39	1.45	2.17	2.09	2.04	1.64	1.53
Lu	0.19	0.23	0.19	0.18	0.19	0.18	0.27	0.27	0.18	0.20	0.29	0.29	0.29	0.23	0.19
Hf	7.3	6.2	5.4	6.0	4.5	4.7	4.0	4.0	5.8	5.0	8.0	8.4	9.4	4.3	4.1
Ta	4.3	2.48	3.4	3.5	2.11	2.46	1.99	1.92	3.29	2.47	1.06	1.02	0.88	2.36	2.37
Pb	5.0	4.1	3.7	4.0	3.6	3.7	4.2	7.3	4.2	3.4	6.8	2.38	4.7	2.94	2.48
Th	7.7	5.9	4.7	4.8	3.4	3.9	4.2	4.3	4.5	3.8	15.3	14.0	11.6	4.2	2.99
U	2.08	1.40	1.22	1.11	0.87	0.98	1.00	1.03	0.94	0.82	3.9	3.8	3.5	1.16	0.79

Abbreviations: Classif. – classification; BA – basaltic andesite; SB – subalkaline basalt; BN – basanite; AB – alkali basalt; HW – hawaiite; KTB – potassic trachybasalt; LOI – loss on ignition.

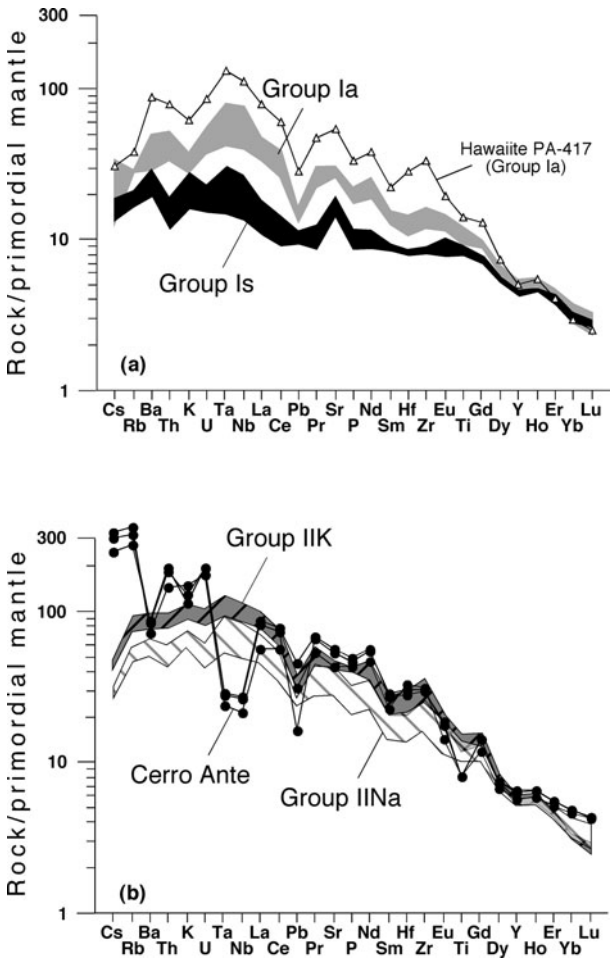

Figure 6. Primordial mantle-normalized incompatible element patterns. (a) Groups Ia and Is; (b) groups IINa, IIK and Cerro Ante. Normalizing values after McDonough & Sun (1995).

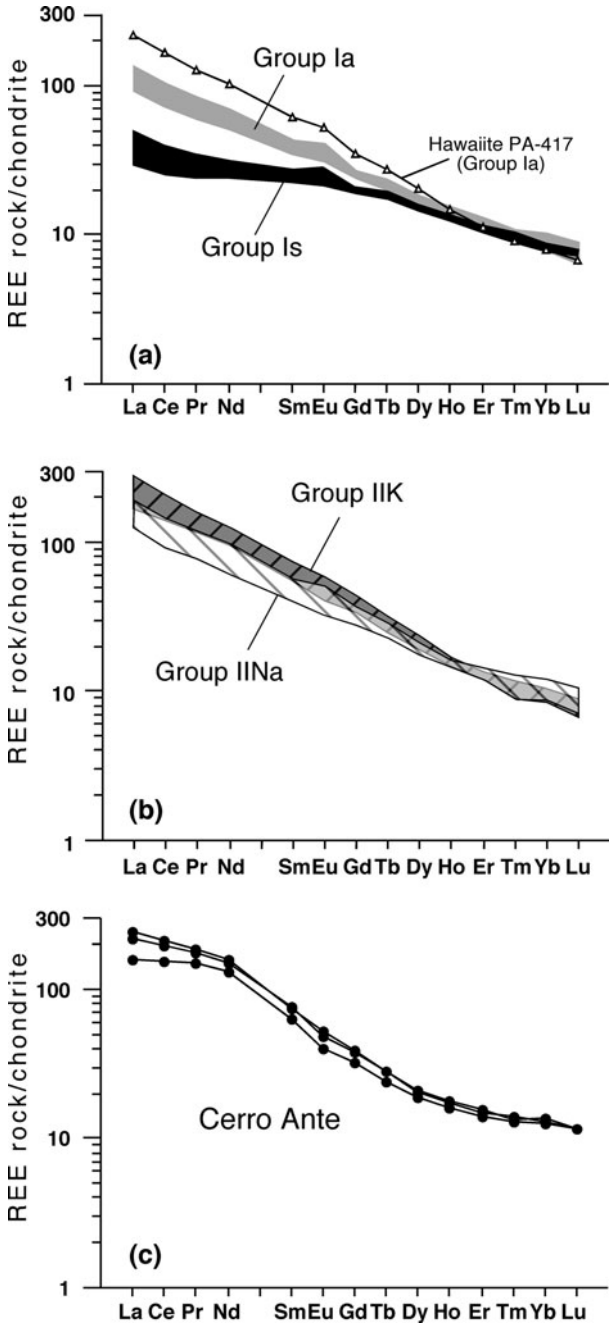

Figure 7. CI chondrite-normalized REE patterns. (a) Groups Ia and Is; (b) groups IINa and IIK; (c) Cerro Ante. Normalizing values after McDonough & Sun (1995).

and a less marked positive Ba anomaly (Fig. 6a). Group Is lavas show less fractionated REE distributions (La_N = 30–50, Yb_N = 7.6–9.0, $(La/Yb)_N$ = 3.6–5.9; Fig. 7a), with LREE less fractionated than HREE ($(La/Sm)_N$ = 1.2–1.9, $(Sm/Yb)_N$ = 2.5–3.2), forming 'kinked' patterns. Samples PA-397 and PA-415 have a slight positive Eu anomaly.

Basanites from Cerro Ante have a completely different incompatible element distribution: the HFS (high field strength) elements Nb, Ta and Ti show marked negative anomalies, the LIL (large ion lithophile) elements Cs, Rb, Th, U and K are strongly enriched, and there is a prominent negative Ba anomaly (Fig. 6b). The concentrations of other elements are comparable to those in group IIK volcanics. The REE patterns (Fig. 7c) are characterized by moderate LREE/HREE fractionation ($(La/Yb)_N$ = 12.3–17.8) and by sigmoidal shapes, with concave-downward LREE and concave-upward HREE. The Pliocene basanite lava from Cerro Gato, analysed by Baker *et al.* (1981) and also located on the western side of the Genoa–Senguerr valley, has a whole-rock chemistry very similar to that of basanites from Cerro Ante.

5. Sr–Nd–Pb isotopes

Seventeen Sr–Nd and fifteen Pb isotope compositions were determined for the studied volcanic rocks (Table 3). Sr–Nd–Pb isotope variability is quite large, and comparable to that of the whole Patagonian Cenozoic magmatic province. Data show a variation in the Sr–Nd isotope composition over time, with a progressive increase in enriched components from the late Eocene to the Pleistocene (Fig. 8). The oldest lavas of group Ia (late Eocene) show the most depleted compositions ($^{87}Sr/^{86}Sr$ = 0.70328–0.70349, $^{143}Nd/^{144}Nd$ = 0.51284–0.51287), close to the extreme values observed for Pali Aike and the

Table 3 Sr–Nd–Pb isotope data

Sample	Age (Ma)	$(^{87}Sr/^{86}Sr)_i$	$(^{143}Nd/^{144}Nd)_i$	$(^{206}Pb/^{204}Pb)_i$	$(^{207}Pb/^{204}Pb)_i$	$(^{208}Pb/^{204}Pb)_i$
PA 425	34.4	0.703489	0.512844	18.846	15.613	38.628
PA 426	*34*	0.703279	0.512867	18.867	15.608	38.601
PA 424	*34*	0.703330	0.512836			
PA 417	22.5	0.703657	0.512763	18.897	15.592	38.647
PA 393	20.6	0.704088	0.512753	18.500	15.604	38.746
PA 394	*20*	0.704237	0.512748	18.638	15.617	38.445
PA 397	19.0	0.704118	0.512755	18.619	15.593	38.394
PA 414	18.6	0.703625	0.512808			
PA 419	18.6	0.704546	0.512685	18.629	15.614	38.491
PAT 71	*2.5*	0.704538	0.512686	18.477	15.588	38.492
PA 400	2.9	0.705788	0.512539	18.171	15.565	38.427
PA 421	2.7	0.704941	0.512665	18.425	15.576	38.462
PA 380	2.6	0.704938	0.512623	18.313	15.569	38.408
PA 409	2.5	0.704872	0.512666	18.255	15.548	38.366
PA 405	*2.5*	0.705014	0.512591	18.318	15.562	38.421
PA 390	1.5	0.704876	0.512747	18.569	15.599	38.491
PA 403	<1	0.705217	0.512578	18.381	15.569	38.456

All ratios are re-calculated back at the time of the eruption of the lavas. Ages in italics are assumed on the basis of geological and geographical relationships with dated rocks.

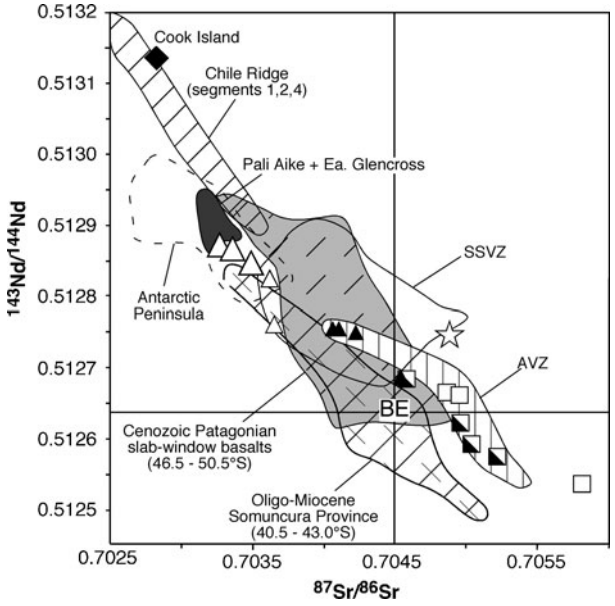

Figure 8. $^{143}Nd/^{144}Nd$ v. $^{87}Sr/^{86}Sr$ plot for the studied samples (symbols as in Fig. 4). Also shown are the fields for the Cenozoic volcanic rocks from the Antarctic Peninsula (Hole, Kempton & Millar, 1993; Hole *et al.* 1995; D'Orazio *et al.* 1999), extra-Andean Patagonia from 46.5 to 50.5° S (Stern *et al.* 1990; Gorring & Kay, 2001; D'Orazio *et al.* 2005; Gorring *et al.* 2003), the Oligo-Miocene Somuncura Province (Kay *et al.* 2007), the Pali Aike volcanic field and Estancia Glencross area (D'Orazio *et al.* 2000, 2001), the Chile Ridge (segments 1, 2, 4; Sturm *et al.* 1999), and the Southern South Volcanic Zone (SSVZ) and Austral Volcanic Zone (AVZ) of the Andes (Hickey, Frey & Gerlach, 1986; Hickey-Vargas *et al.* 1989; Futa & Stern, 1988; Gerlach *et al.* 1988; López-Escobar *et al.* 1993, 1995; Stern & Kilian, 1996; D'Orazio *et al.* 2003). BE – Bulk Earth.

Estancia Glencross area (~ 52° S; D'Orazio *et al.* 2000, 2001). Early Miocene lavas (group Is and part of group Ia) plot in the central part of the array defined by the studied samples, with $^{87}Sr/^{86}Sr$ and $^{143}Nd/^{144}Nd$ ranging from 0.70364 to 0.70455 and from 0.51269 to 0.51282, respectively. The Plio-Pleistocene lavas (groups IIK and IINa) show the most enriched Sr–Nd isotope compositions ($^{87}Sr/^{86}Sr$ = 0.70454–0.70579; $^{143}Nd/^{144}Nd$ = 0.51254–0.51268), and some samples are the most isotopically enriched of the whole Patagonian Cenozoic magmatic province. The basanite sample from Cerro Ante plots to the right of the array defined by the other groups; it has a relatively high $^{87}Sr/^{86}Sr$ ratio (0.70488) and a $^{143}Nd/^{144}Nd$ ratio (0.51275) that falls within the values observed for the early Miocene lavas and for the volcanic rocks of the Southern South Volcanic Zone of the Andes.

In the $^{207}Pb/^{204}Pb$ and $^{208}Pb/^{204}Pb$ v. $^{206}Pb/^{204}Pb$ (Fig. 9a, b) isotope diagrams, Sierra de San Bernardo lavas plot above the Northern Hemisphere Reference Line (Hart, 1984) and largely overlap with the other Cenozoic Patagonian lavas from southern and northern Patagonia (Stern *et al.* 1990; Gorring & Kay, 2001; Gorring *et al.* 2003; Kay *et al.* 2007). The variability of the $^{206}Pb/^{204}Pb$ ratio (18.17–18.90) is much larger than that of $^{207}Pb/^{204}Pb$ (15.55–15.62) and $^{208}Pb/^{204}Pb$ (38.37–38.75). Again, we observe a time-related distribution of the Pb isotope composition. Group Ia lavas have the highest $^{206}Pb/^{204}Pb$ ratios and fall close to the Northern Hemisphere Reference Line and to the extreme values of Pali Aike basalts, filling the gap between the latter and other Patagonian basalts. The lowest $^{206}Pb/^{204}Pb$ ratios have been measured in group IIK volcanic rocks. Similar Pb isotope compositions also characterize the Plio-Pleistocene 'post-plateau' lavas from Meseta del Lago Buenos Aires (Gorring *et al.* 2003). The sample from Cerro Ante ($^{206}Pb/^{204}Pb$ = 18.57) plots between group Is and groups IIK/IINa, and within the field of the calc-alkaline volcanic rocks from the Southern South Volcanic Zone of the Andes. The $^{87}Sr/^{86}Sr$ v. $^{206}Pb/^{204}Pb$ plot (Fig. 10) highlights the isotopic similarities between group Ia basalts and basalts from Pali Aike and the Antarctic Peninsula.

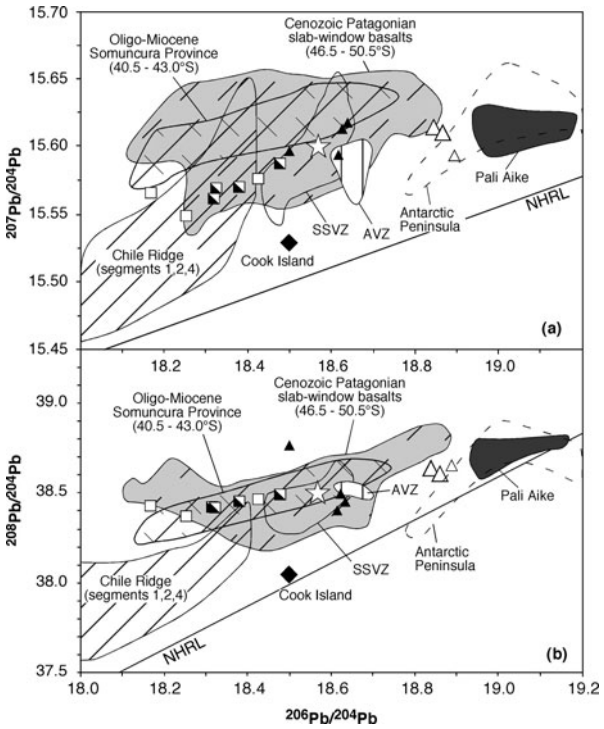

Figure 9. $^{207}Pb/^{204}Pb$ v. $^{206}Pb/^{204}Pb$ (a) and $^{208}Pb/^{204}Pb$ v. $^{206}Pb/^{204}Pb$ (b) plots for the studied samples (symbols as in Fig. 4). The diagram also shows the Northern Hemisphere Reference Line (NHRL; Hart, 1984). Data sources and abbreviations: see Figure 8 caption.

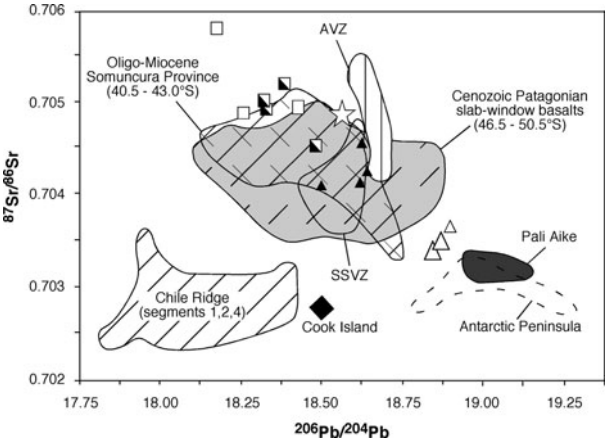

Figure 10. $^{87}Sr/^{86}Sr$ v. $^{206}Pb/^{204}Pb$ plot for the studied samples (symbols as in Fig. 4). Data sources and abbreviations: see Figure 8 caption.

6. Discussion

6.a. Evaluation of crustal contamination processes

Mantle-derived magmas rising through the continental crust are susceptible to varying degrees of contamination by crustal materials. Before discussing the nature of the mantle sources of Sierra de San Bernardo magmas, we therefore need to assess how crustal inputs affect their chemistry and isotope composition. The basanites from Cerro Ante are subaphyric rocks characterized by high Mg numbers (71–72) and high Ni (175–220 ppm) and Cr (475–505 ppm) concentrations, which are indicative of negligible contamination by crustal materials during upwelling. The lavas of the other groups have elemental ratios which are more sensitive to upper crustal contamination (e.g. K/P, Rb/Nb, Pb/Nb, Th/La), with values that differ considerably from those of the average upper continental crust (Taylor & McLennan, 1995) but are very close to those of the average E-MORB (Enriched Mid Ocean Ridge Basalts) and OIB (Ocean Island Basalts; Sun & McDonough, 1989; Fig. 11). The Jurassic Chon Aike rhyolites, a voluminous and widespread upper crustal component of Patagonia (Pankhurst & Rapela, 1995), are even more unlikely contaminants of Sierra de San Bernardo magmas, since they are characterized by much higher LILE/HFSE ratios. A further argument against contamination of Sierra de San Bernardo magmas by upper crustal materials is the lack of positive correlation between their degree of evolution and values of elemental ratios sensitive to crustal contamination.

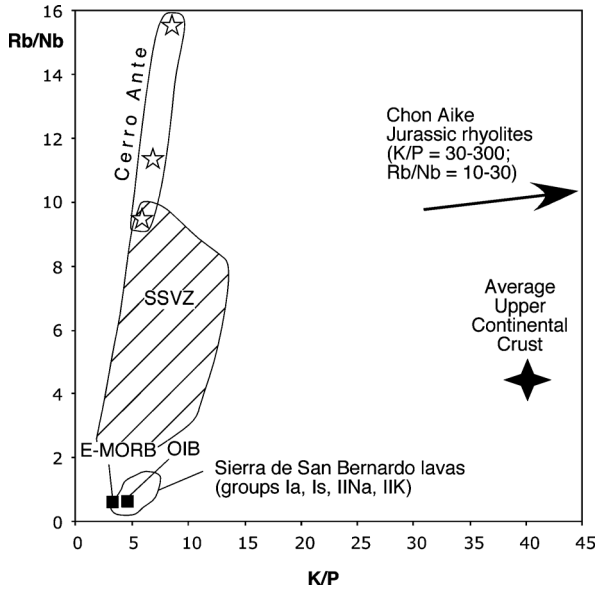

Figure 11. Rb/Nb v. K/P plot for the studied samples. The diagram also shows the field for the Southern South Volcanic Zone of the Andes (SSVZ) volcanic rocks with MgO > 3 wt %, the average values for E-MORB and OIB (Sun & McDonough, 1989), the average value of the Upper Continental Crust (Taylor & McLennan, 1995), and the range for the Chon Aike Jurassic rhyolites (Pankhurst & Rapela, 1995).

As stressed in the results sections, the early Miocene subalkaline lavas (group Is) are characterized by relatively low Mg numbers and Ni concentrations, coupled with low concentrations of most incompatible elements except Sr and Ba, which form positive spikes in the mantle-normalized plots (Fig. 6a). Moreover, these lavas have more enriched Sr and Nd isotope compositions with respect to the coeval or older alkaline lavas of group Ia. These compositional features are compatible with a process of crystal fractionation of mafic phases coupled with an assimilation of felsic materials from the lower continental crust. It is difficult to test the case for a lower crust contamination of

group Is lavas, as we know neither the composition of group Is magmas before the supposed contamination nor the nature of the lower crust under the study area. Nonetheless, we tried to test this hypothesis using the energy-constrained assimilation and fractional crystallization (EC-AFC) model of Spera & Bohrson (2001). The lower continental crust contaminant was obtained by averaging the compositions of the mafic granulite xenoliths from Sierra de los Chacays (southern Meseta de Somuncura, ~ 42.5° S 68° W: Pankhurst & Rapela, 1995). Calculation results indicate that starting from a model subalkaline primary melt with the Sr/Nd, $^{87}Sr/^{86}Sr$ and $^{143}Nd/^{144}Nd$ ratios of group Ia lavas, ~ 20 wt % crystal fractionation of mafic phases coupled with 0.4–0.8 wt % assimilation of lower crust melts reproduce quite well the $^{87}Sr/^{86}Sr$ and Sr/Nd ratios of group Is lavas (Fig. 12a). However, the $^{143}Nd/^{144}Nd$ ratios of group Is can only be reproduced starting from the sample of group Ia with the lowest $^{143}Nd/^{144}Nd$ ratio (Fig. 12b).

In summary, based on isotopic and trace element data, we conclude that none of the alkaline magmas from the study area suffered any detectable contamination by materials from the Patagonian continental crust, whereas the chemical and isotopic features of group Is subalkaline basalts and basaltic andesites do not allow us to exclude a slight contamination by lower crust melts, possibly during magma ponding and crystallization at the base of the continental crust.

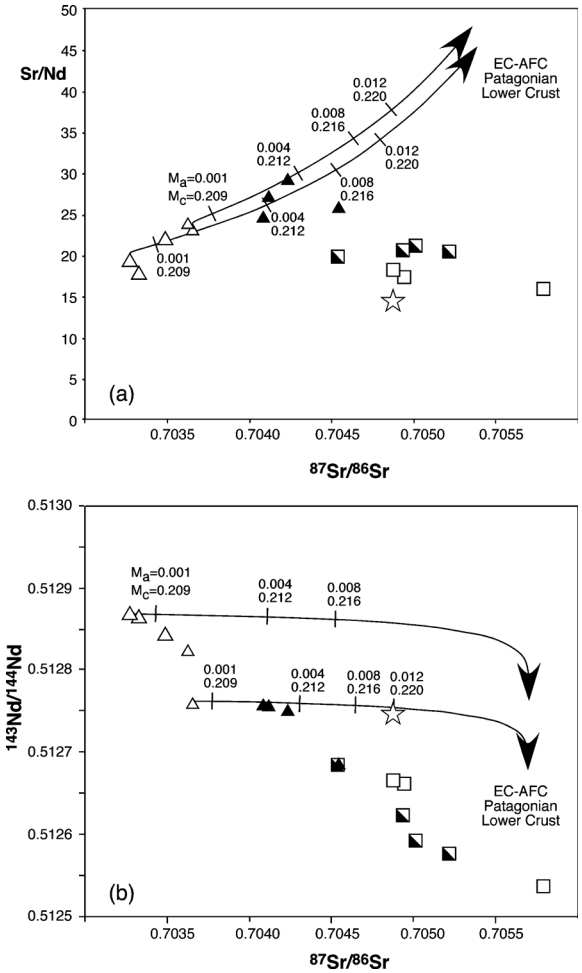

Figure 12. Sr/Nd v. $^{87}Sr/^{86}Sr$ (a) and $^{143}Nd/^{144}Nd$ v. $^{87}Sr/^{86}Sr$ (b) plots showing the results of EC-AFC (energy constrained-assimilation fractional crystallization) modelling (Spera & Bohrson, 2001; symbols as in Fig. 4). The Patagonian lower crust contaminant (Sr = 625 ppm, Nd = 4.1 ppm, $^{87}Sr/^{86}Sr$ = 0.70695, $^{143}Nd/^{144}Nd$ = 0.51237) was estimated by averaging the compositions of mafic granulite xenoliths from Sierra de los Chacays (Pankhurst & Rapela, 1995). The basalt magma composition before contamination was approximated assuming that it had the REE concentrations (Nd = 8.5 ppm) of a subalkaline silicate melt obtained by 15 % partial melting of a garnet-bearing pyrolite source, and Sr/Nd, $^{87}Sr/^{86}Sr$ and $^{143}Nd/^{144}Nd$ ratios of group Ia lavas. In particular, in the calculations we selected Eocene sample PA-426, characterized by the most depleted Sr–Nd isotope composition and, as an alternative, Miocene sample PA-417, showing the most enriched Sr–Nd isotope composition. Thermal and thermodynamic parameters and bulk partition coefficients for Nd and Sr are those used by Spera & Bohrson (2001) for their lower crust assimilation example, except for the Sr bulk partition coefficient in the crystallizing basalt magma, that has been taken equal to 0.05. Numbers on tick marks are the mass of assimilated material (M_a) and the mass of cumulates (M_c), respectively, both referred to a unitary mass of initial magma.

6.b. Time–depth evolution of mantle sources of Sierra de San Bernardo magmas

A major finding of this study is the large time-related variation in the Sr–Nd–Pb isotope composition of Sierra de San Bernardo lavas (Figs. 8–10). From the late Eocene to the Pleistocene, magmas with progressively lower $^{143}Nd/^{144}Nd$ and $^{206}Pb/^{204}Pb$ and higher $^{87}Sr/^{86}Sr$ ratios were erupted. These time-related isotopic variations are not associated with corresponding regular variations in the chemistry of the lavas. Indeed, moderate- to low-degree melting during late Eocene, Miocene, Pliocene and Pleistocene times produced alkaline magmas, whereas high-degree melting was restricted to the Miocene and produced subalkaline magmas.

Though characterized by different Sr–Nd–Pb isotope compositions and ages, group Ia, IIK and IINa alkaline basalts, trachybasalts and basanites show similar incompatible element distributions (Fig. 6a, b). These distributions are common among the alkaline mafic lavas in many volcanic fields of central and southern Patagonia and are generally interpreted as the result of moderate- to low-degree (1–6 %) melting of a slightly enriched mantle source, leaving garnet in the solid residue (Gorring *et al.* 1997; Espinoza *et al.* 2005; Massaferro *et al.* 2006). The MgO contents and Mg numbers for the alkaline lavas, excluding those contaminated by disaggregated ultramafic xenoliths and the basanites from Cerro Ante, are too low to be in equilibrium with mantle olivine (~ Fo_{90}), indicating that they lost olivine (the main or only phenocryst phase) during their ascent. The composition of the primary magmas was restored by continuously adding equilibrium olivine to the lavas until they were in equilibrium with olivine Fo_{90} (Pearce, 1978). In the calculation, the K_D $(Fe/Mg)^{ol/liq}$ was taken as constant

and equal to 0.30. Results indicate that the amount of added olivine varies between 12 and 23 wt %. Though affected by uncertainties linked to model assumptions, the compositions of the calculated primary magmas can be profitably used to make a relative estimate of the pressure of their last equilibration with the mantle. We here used the equation proposed by Albarede (1992), which is based on the SiO_2 and MgO content of the primary liquid. Results show that the alkaline primary melts were originated at variable pressures of 1.6 to 3.6 GPa, with the late Eocene magmas equilibrating at the highest pressures (2.7–3.6 GPa). The pressure interval obtained in the calculations is consistent with the occurrence of residual garnet in the source, as expected on the basis of LREE/HREE fractionation in the alkaline lavas, which indicates pressures in excess of 2.0 GPa (Klemme & O'Neill, 2000). The higher equilibration pressures estimated for the late Eocene lavas are also in agreement with their higher iron contents, which, as experimental data suggest, increase with melting pressure (Hirose & Kushiro, 1993). The transition from lavas with high $^{143}Nd/^{144}Nd$ and $^{206}Pb/^{204}Pb$ and low $^{87}Sr/^{86}Sr$ (late Eocene) to lavas with high $^{87}Sr/^{86}Sr$ and low $^{143}Nd/^{144}Nd$ and $^{206}Pb/^{204}Pb$ (Plio-Pleistocene) is related to a vertical mantle heterogeneity with domains characterized by more radiogenic Sr and less radiogenic Nd and Pb residing at shallower levels.

It is more difficult to evaluate the melting pressures of primary magmas parental to the group Is subalkaline lavas. As shown before, these rocks have more differentiated major element compositions but lower incompatible element concentrations with respect to the alkaline lavas, and Sr–Nd–Pb isotope compositions intermediate between those of group Ia and groups IIK and IINa. In the previous paragraph we showed that the assimilation of lower crust materials cannot be excluded, justifying, at least in part, some of their compositional features.

In accordance with experimental data (e.g. Kushiro, 2001), the silica-oversaturated nature of these basalts suggests that they segregated from the peridotite mantle at pressures of 1.0–1.5 GPa. On the other hand, their HREE fractionation ($(Sm/Yb)_N$ = 2.5–3.2), indicative of garnet in the solid residue during partial melting, implies pressures in excess of 2.0 GPa (Klemme & O'Neill, 2000). This apparent paradox has been previously reported for subalkaline basalts occurring in other parts of the world (e.g. Hawaii: Wagner & Grove, 1998; southern Patagonia: D'Orazio *et al.* 2001; northeastern China: Xu *et al.* 2005) and interpreted as an effect of the reaction between an upwelling primary basalt magma, originated by partial melting of a garnet–lherzolite, and the shallower lithospheric mantle. Besides reconciling the above-mentioned melting depths paradox, this kind of reaction process can also account for the anomalously high Cr/Ni ratios and silica-oversaturation of group Is lavas. During the reaction process, the magma crystallizes olivine (lower SiO_2 and Cr/Ni) and dissolves pyroxene (higher SiO_2 and Cr/Ni), thus increasing its silica saturation and Cr/Ni ratios. As shown by the numerical plate models developed by Vernieres, Godard & Bodinier (1997), basalt melt/peridotite reactions are also able to reproduce the peculiar 'kinked' REE pattern of group Is lavas.

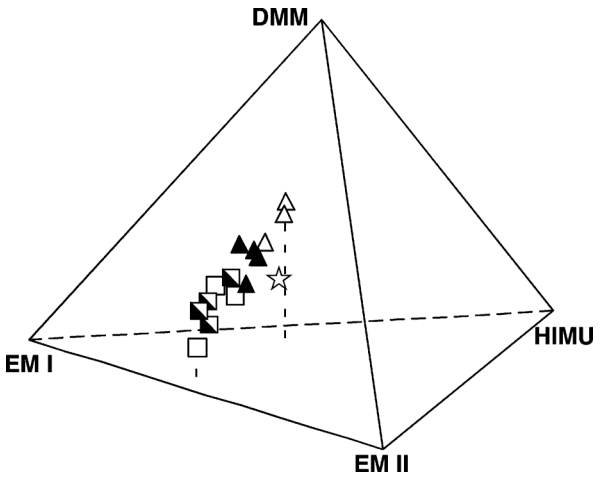

Figure 13. Three-dimensional plot of $^{87}Sr/^{86}Sr$, $^{143}Nd/^{144}Nd$ and $^{206}Pb/^{204}Pb$ for Sierra de San Bernardo and Cerro Ante samples, using the four end-members DMM, EM I, EM II and HIMU at the vertices of the tetrahedron (end-member compositions after Hart *et al.* 1992; symbols as in Fig. 4).

6.c. Asthenospheric v. lithospheric mantle sources

The Sr–Nd–Pb isotope compositions of Sierra de San Bernardo lavas clearly indicate that different mantle reservoirs were progressively activated from the late Eocene to the Pleistocene. When plotted in the compositional tetrahedron which has at its vertices the $^{87}Sr/^{86}Sr$, $^{143}Nd/^{144}Nd$, $^{206}Pb/^{204}Pb$ of the four HIMU-DMM-EM I-EM II end-members (Fig. 13; Hart *et al.* 1992), Sierra de San Bernardo data form a linear array whose extremes fall close to the HIMU-DMM-EM I face (group Ia) and the EM I–EM II edge (group IIK), respectively. In accordance with their higher depth of equilibration and their Sr–Nd–Pb isotope features, the oldest alkaline magmas (group Ia) are believed to be sourced within the asthenospheric mantle. This conclusion is sustained by the close similarity between group Ia lavas and the Neogene basalts from Pali Aike, the Estancia Glencross area and the Antarctic Peninsula, which have been interpreted as more or less pure asthenospheric melts (Hole, Kempton & Millar, 1993; Hole *et al.* 1995; D'Orazio *et al.* 2000, 2001). Note that the isotopic features of this subcontinental asthenosphere strongly contrast with those of the suboceanic asthenosphere sampled by the Chile Ridge basalts (Figs. 8–10). Indeed, the latter have MORB-like Sr–Nd–Pb isotope compositions ($^{87}Sr/^{86}Sr$ = 0.7024–0.7036, $^{143}Nd/^{144}Nd$ = 0.5129–0.5132 and $^{206}Pb/^{204}Pb$ = 17.8–18.4: Sturm *et al.* 1999).

The Miocene subalkaline lavas and the subsequent Plio-Pleistocene alkaline lavas were derived from

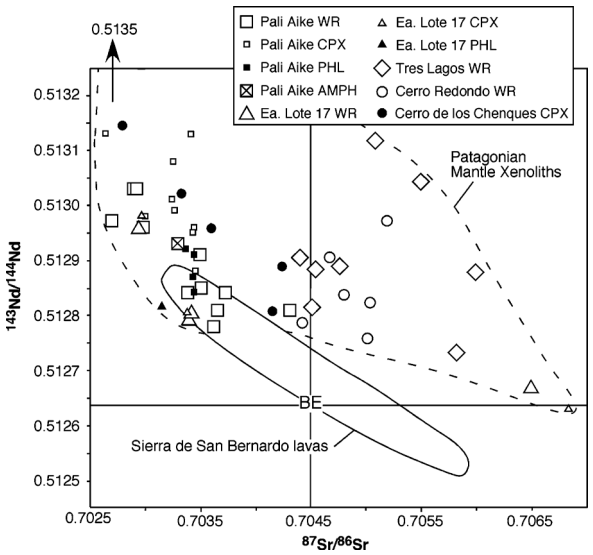

Figure 14. $^{143}Nd/^{144}Nd$ v. $^{87}Sr/^{86}Sr$ plot for Patagonian mantle xenoliths. Data sources: Pali Aike: Stern *et al.* (1999) and Kempton *et al.* (1999); Estancia Lote 17: Gorring & Kay (2000) and Conceição *et al.* (2005); Cerro Redondo: Schilling *et al.* (2005); Tres Lagos: Ntaflos *et al.* (2007); Cerro de los Chenques: Rivalenti *et al.* (2007). Abbreviations: WR – whole rock; CPX – clinopyroxene; PHL – phlogopite; AMPH – amphibole.

mantle sources containing an enriched component characterized by high $^{87}Sr/^{86}Sr$ (> 0.7055) and low $^{143}Nd/^{144}Nd$ (< 0.5126) and $^{206}Pb/^{204}Pb$ (< 18.2) ratios. The contribution of this component increased with time and with the degree of alkalinity of the erupted lavas. This enriched component, isotopically akin to the EM I mantle, is considered to be stored within the lower portions of the Patagonian lithospheric mantle (Gorring *et al.* 2003). The Sr–Nd isotope compositions of Patagonian mantle xenoliths (e.g. Schilling *et al.* 2005; Rivalenti *et al.* 2007 and references therein) indicate that the mantle lithosphere is isotopically heterogeneous (Fig. 14). Nonetheless, depleted compositions prevail, suggesting a recent (late Proterozoic–early Phanerozoic) stabilization of the subcontinental mantle from a MORB-source-type asthenosphere (Stern *et al.* 1999). The enriched lithospheric domains that we consider responsible for the geochemical features of groups Is, IINa and IIK were not frequently sampled as mantle xenoliths, possibly because they are seated at deeper levels close to the asthenosphere–lithosphere transition or because they are dispersed in a prevailing isotopically depleted mantle matrix.

In summary, according to our data, the late Eocene to Pleistocene basaltic rocks from the Sierra de San Bernardo record the progressive transition from mantle melting confined within the asthenosphere to mantle melting involving deep and enriched lithospheric domains whose role increases through time.

6.d. Petrogenesis of the basanites from Cerro Ante

The Pleistocene basanite lavas from Cerro Ante show some peculiar chemical features that set them apart from the other basaltic rocks in the study area. Particularly striking are the pronounced negative Ta and Nb anomalies (and the less marked negative Ti anomaly), the strong enrichment in alkaline elements (Cs, Rb and to a lesser extent K) and the negative Ba anomaly ($Ba/Ba^* = 0.3–0.4$; $Ba/Ba^* = Ba_N/(Rb_N{}^*Th_N)^{1/2}$). One sample (PA-390) almost satisfies the chemical criteria for defining a rock as ultrapotassic (Foley *et al.* 1987). The sigmoidal shape of the REE patterns is also peculiar, with LREE and HREE much less fractionated than the middle REE. The Sr–Nd–Pb isotope composition is similar to that of the volcanic rocks from the Southern South Volcanic Zone of the Andes, but is also very close to the most common values for Cenozoic basalts from southern Patagonia. It is also noteworthy that the lavas from Cerro Ante have reasonably low Ti/V ratios (37–38), as expected for subduction-related magmas (Shervais, 1982). Indeed, the Ti/V ratios are intermediate between those of the basalt and basaltic andesite lavas from Cay and Maca volcanoes ($Ti/V = 25 \pm 3$: D'Orazio *et al.* 2003), located on the active magmatic arc at approximately the same latitude as Cerro Ante, and those of the large majority of the other Cenozoic mafic lavas from the study area and southern Patagonia ($Ti/V = 50–100$). However, Cerro Ante lavas display negative Pb anomalies, in contrast with the volcanic rocks from the nearby Southern South Volcanic Zone of the Andes where Pb forms marked positive spikes (e.g. Cay and Maca volcanoes: D'Orazio *et al.* 2003). Lastly, their CaO/Al_2O_3 wt % ratio (~ 0.70) is higher than that of Sierra de San Bernardo lavas (0.58 ± 0.07).

Whatever the melting mineral assemblage and the melting mode, a pyrolite or a more depleted mantle rock cannot be the source of the LILE-enriched basanites from Cerro Ante, even at extremely low (< 1 %) degrees of melting. A mantle that is strongly enriched in Cs, Rb, K, Th, U and LREE is clearly needed for the generation of these magmas. While the high LILE/HFSE and low Ti/V ratios are typical of mantle sources metasomatized by subduction-derived materials, the negative Pb anomalies and the low Ba/Ba^* values require additional explanations. Lead is one of the most mobile elements in aqueous fluids (Kogiso, Tatsumi & Nakano, 1997), thus, it can be more efficiently removed from the subducting slab beneath the Andean forearc and active volcanic arc with respect to the other fluid mobile elements, leaving the subducted material beneath the back-arc region strongly Pb-depleted. Assuming a constant slab dip in the 0–400 km space interval from the trench, and a depth of the slab top under the active volcanic arc of 110 km (corresponding to a slab dip of $\sim 29^\circ$), we estimate that the top of the subducted slab beneath Cerro Ante should be located at a depth of about 190 km (~ 6 GPa). Hydrous silicate phases stable in this deep part of the slab or the immediately overlying mantle wedge, such as phlogopite and K-richterite (Sudo & Tatsumi, 1990), have variable

partition coefficients for the LILE but $D_{Rb}/D_{Ba} > 1$ (Plá Cid *et al.* 2005; Tiepolo *et al.* 2003). Low-degree melts or fluids released from these materials would be able to metasomatize a portion of the overlying mantle whose succesive partial melting may produce the peculiar geochemical features of Cerro Ante basanites.

The subduction-related origin of the Cerro Ante magmas is in agreement with the geological setting of this small volcanic occurrence on the easternmost slopes of the Andean foothills, in the westernmost part of the study area (Fig. 2). The paucity of lavas with these geochemical features has to be linked to the tectonic setting of the Andean foothills that allows the ascent of deep-seated magmas only in very confined areas.

6.e. Sierra de San Bernardo magmatism and geodynamic evolution

Current knowledge of intra-continental, Cenozoic basaltic magmatism in Patagonia strongly suggests that it originated neither in relation to a high heat flux mantle plume nor in relation to significant regional-scale lithospheric extension (Ramos & Kay, 1992). The cause of widespread mantle melting under this area during the Cenozoic thus remains unresolved.

To the southeast of the modern Chile Triple Junction, the genesis of basaltic magmas has been ascribed to the middle Miocene to Present opening of a slab window (Ramos & Kay, 1992; Gorring *et al.* 1997; D'Orazio *et al.* 2000, 2001, 2005; Gorring & Kay, 2001; Gorring *et al.* 2003; Espinoza *et al.* 2005). Within this tectonic framework, mantle melting occurs as the hot sub-slab asthenosphere rises to fill the space left by the diverging subducting plates and crosses its solidus by adiabatic decompression. According to some authors (Ramos & Kay, 1992; Espinoza *et al.* 2005), mantle melting and basalt effusion related to slab window opening occurred several times in Patagonia as a consequence of Neogene, Palaeogene and even older ridge–trench collisions. Guivel *et al.* (2006) alternatively proposed that beneath the Meseta Chile Chico–Meseta del Lago Buenos Aires area, the sub-slab asthenospheric mantle rose up through a tear-in-the-slab formed starting from *c.* 15 Ma. The Sierra de San Bernardo is located outside (north of) the vertical projection of the supposed middle Miocene to Present slab window; however, the Plio-Pleistocene basalts were erupted just about 50 to 150 km north of the northernmost slab window edge. This relatively short distance from the slab window does not preclude at least a thermal influence of this latter on the genesis of the most recent basalts from Sierra de San Bernardo. The limited amount of palaeomagnetic data on Pacific oceanic crust predating the Miocene does not allow us to constrain accurately the space–time evolution of the Palaeogene slab-window, but it is very likely that at the time the first basalts were erupted in the Sierra de San Bernardo (late Eocene), the slab window had already migrated to more southern latitudes (Cande & Leslie, 1986).

Several models have been put forward to explain the upwelling and melting of the asthenosphere under northern Patagonia: de Ignacio *et al.* (2001) proposed that a combination of slab roll-back, the curved (concave-up) topography of the subducted slab, and late Oligocene plate reorganization favoured the intake of hot asthenospheric mantle under the Meseta de Somuncura area (northern Patagonia). As an alternative, Kay *et al.* (2007) attributed the Oligocene–Miocene magmatism of the same area to asthenosphere upwelling due to thermal instability in the mantle associated with the late Oligocene change in the convergence vectors of the Pacific oceanic plates with respect to South America.

Reconstructed global absolute plate motions suggest a generalized 'westward' drift of lithosphere relative to the underlying mantle (e.g. Scoppola *et al.* 2006 and references therein). In the hotspot reference frame (Gripp & Gordon, 2002), the South American Plate is moving westward relative to the mantle. Assuming that the main mantle–lithosphere décollement surface is located in the Low-Velocity Zone (Thybo, 2006), we suppose that the relative eastward-directed mantle flow involves the sub-lithospheric mantle, whereas the mantle wedge sandwiched between lower and upper converging plates is shielded and free to move westward along with the upper plate (Fig. 15). As a consequence, the space created by this motion is compensated by the upwelling of mantle. In this framework, the upwelling asthenospheric mantle melted by decompression, producing the late Eocene–early Miocene alkaline magma (group Ia; Fig. 15a). The melting source eventually moved upward, thereby involving the lower part of the lithospheric mantle and originating the Miocene to Pleistocene basaltic magmas with an enriched Sr–Nd isotope signature (Fig. 15b).

7. Summary and conclusions

The study of the mafic volcanic rocks from the Sierra de San Bernardo and neighbouring areas allows us to discuss the time-evolution of the sources of Cenozoic magmatism in central Patagonia in the framework of the geodynamic evolution of southern South America. Based on K–Ar geochronology, bulk chemistry and Sr–Nd–Pb isotope data we conclude that:

(1) The studied rocks can be subdivided into five groups: group Ia consists of alkaline mafic lavas (basanites, alkali basalts, trachybasalts) erupted during the late Eocene and early Miocene; group Is comprises quartz-normative lavas (subalkaline basalts, basaltic andesites) erupted exclusively during the early Miocene; groups IIK and IINa are alkaline Plio-Pleistocene lavas (basanites, alkali basalts, trachybasalts) discriminated on the basis of their K_2O/Na_2O ratios; the Pleistocene basanite lavas from the Cerro Ante monogenetic cone (located on the easternmost slopes of the Patagonian Andes)

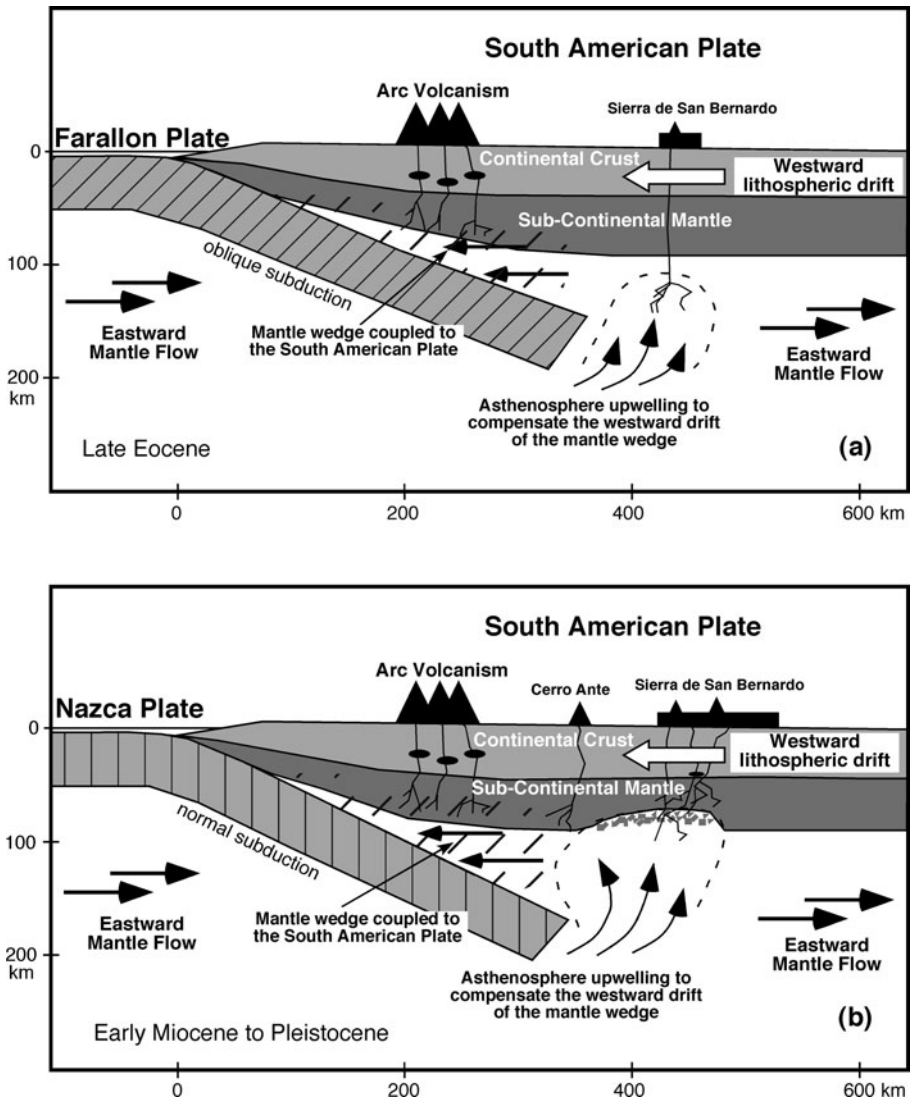

Figure 15. Schematic illustration showing the geodynamic model for Cenozoic mafic magmatism in central Patagonia. (a) Magmatism started during the late Eocene, when the asthenosphere welled up to compensate for the westward drift of the mantle wedge associated with the South American Plate and melted by adiabatic decompression. (b) Progressive lithospheric erosion induced by the upwelling of the asthenospheric mantle activated more isotopically enriched sources that produced the subsequent Miocene, Pliocene and Pleistocene lavas. The Pleistocene lavas from Cerro Ante, located between the Andean Arc and Sierra de San Bernardo, were sourced from a mantle domain extensively modified by subduction-related components (hatched area).

have a marked orogenic geochemical affinity that sets them apart from the other lavas.

(2) The Sr–Nd–Pb isotope compositions and bulk chemical compositions of the late Eocene to early Miocene alkaline group Ia lavas match those of the asthenospheric magmas erupted in the Pali Aike Volcanic Field, in the Estancia Glencross area (southernmost Patagonia, Miocene–Recent) and in the Antarctic Peninsula (Miocene to Recent). Moreover, their compositions indicate a deeper level of equilibration in the mantle with respect to subsequent lavas. Accordingly, we suggest a dominantly asthenospheric origin for these magmas.

(3) The chemical and isotopic features of the early Miocene group Is subalkaline lavas are indicative of high-degree melting at depth, followed by reaction between the melt and the overlying lithospheric mantle. Some chemical peculiarities of these lavas also suggest a small input of lower crustal melts.

(4) The more recent alkaline lavas of groups IIK and IINa are among the most enriched in terms of Sr–Nd isotope composition of all of extra-Andean Patagonia. Their occurrence is due to the activation, possibly in relation to local extensional tectonic processes, of enriched lithospheric domains at the lithosphere–asthenosphere boundary.

(5) The basanites from Cerro Ante originated in the near back-arc of the Andes from a mantle source extensively modified by the addition of low-degree melts or fluids released from the deep portion of the subducting slab or from the metasomatized mantle immediately overlying the slab.

(6) The progressive involvement of enriched lithospheric mantle domains in the genesis of the studied lavas from the late Eocene to the Pleistocene reveals a process of lithospheric erosion induced by the upwelling of asthenospheric mantle beneath the study area. Based on current knowledge about the relative movement and decoupling between lithosphere and asthenosphere, we propose that the asthenosphere under the study area rose up to compensate the westward drift of the mantle wedge associated with the South American lithosphere.

Acknowledgements. The authors wish to thank Carlo Doglioni for the critical reading of the manuscript and the fruitful discussions, Marco Bertoli and Marco Tamponi for XRF analyses, Riccardo Vannucci and Matthew L. Gorring for their constructive reviews, and David Pyle for the editorial assistance. This research was funded by MIUR-ITALY and by the Italian National Antarctic Research Program (PNRA).

References

ALBAREDE, F. 1992. How deep do common basaltic magmas form and differentiate? *Journal of Geophysical Research* **97**, 10997–11009.

BAKER, P. E., REA, W. J., SKARMETA, J., CAMINOS, R. & REX, D. C. 1981. Igneous history of the Andean cordillera and Patagonian plateau around latitude 46°S. *Philosophical Transactions of the Royal Society of London* **A303**, 105–49.

BALOGH, K. 1985. K–Ar dating of Neogene volcanic activity in Hungary. Experimental technique, experiences and methods of chronological studies. *ATOMKI* Rep. D/1, pp. 277–88.

CANDE, S. C. & LESLIE, R. B. 1986. Late Cenozoic tectonics of the Southern Chile Trench. *Journal of Geophysical Research* **91**, 471–96.

CEMBRANO, J., HERVÉ, F. & LAVENU, A. 1996. The Liquiñe-Ofqui fault zone: a long-lived intra-arc fault system in southern Chile. *Tectonophysics* **259**, 55–66.

CHELOTTI, L. A. 1997. Evolución tectónica de la Cuenca del Golfo San Jorge en el Cretácico y Terciario; algunas observaciones desde la interpretación sísmica. *Boletín de Informaciones Petroleras* **49**, 62–82.

CONCEIÇÃO, R. V., MALLMANN, G., KOESTER, E., SCHILLING, M., BERTOTTO, G. W. & RODRIGUEZ-VARGAS, A. 2005. Andean subduction-related mantle xenoliths: isotopic evidence of Sr–Nd decoupling during metasomatism. *Lithos* **82**, 273–87.

DE IGNACIO, C., LÓPEZ, I., OYARZUN, R. & MÁRQUEZ, A. 2001. The northern Patagonia Somuncura plateau basalts: a product of slab-induced, shallow asthenospheric upwelling? *Terra Nova* **13**, 117–21.

D'ORAZIO, M., AGOSTINI, S., INNOCENTI, F., HALLER, M. J., MANETTI, P. & MAZZARINI, F. 2001. Slab window-related magmatism from southernmost South America: the late Miocene mafic volcanics from the Estancia Glencross area (~52°S, Argentina–Chile). *Lithos* **57**, 67–89.

D'ORAZIO, M., AGOSTINI, S., MAZZARINI, F., INNOCENTI, F., MANETTI, P., HALLER, M. J. & LAHSEN, A. 2000. The Pali Aike Volcanic Field, Patagonia: slab-window magmatism near the tip of South America. *Tectonophysics* **321**, 407–27.

D'ORAZIO, M., GONZALEZ-FERRÁN, O., INNOCENTI, F., MAZZARINI, F., MAZZUOLI, R., TONARINI, S. & ADORNI-BRACCESI, A. 1999. Alkaline basaltic volcanism in the Weddell Sea side of the northernmost Antarctic Peninsula: Sr–Nd isotope and trace-element characteristics. *8th International Symposium on Antarctic Earth Sciences, Wellington, Abstract volume*, p. 92.

D'ORAZIO, M., INNOCENTI, F., MANETTI, P. & HALLER, M. J. 2004. The Cenozoic back-arc magmatism of the southern extra-Andean Patagonia (44.5–52°S): A review of geochemical data and geodynamic interpretations. *Revista de la Asociación Geológica Argentina* **59**, 525–38.

D'ORAZIO, M., INNOCENTI, F., MANETTI, P., HALLER, M. J., DI VINCENZO, G. & TONARINI, S. 2005. The Late Pliocene mafic lavas from the Camusú Aike Volcanic Field (~50°S, Argentina): evidences for geochemical variability in slab window magmatism. *Journal of South American Earth Sciences* **18**, 107–24.

D'ORAZIO, M., INNOCENTI, F., MANETTI, P., TAMPONI, M., TONARINI, S., GONZÁLEZ-FERRÁN, O., LAHSEN, A. & OMARINI, R. 2003. The Quaternary calc-alkaline volcanism of the Patagonian Andes close to the Chile Triple Junction: geochemistry and petrogenesis of volcanic rocks from the Cay and Maca volcanoes (~45°S, Chile). *Journal of South American Earth Sciences* **16**, 219–42.

ESPINOZA, F., MORATA, D., PELLETER, E., MAURY, R. C., SUÁREZ, M., LAGABRIELLE, Y., POLVÉ, M., BELLON, H., COTTEN, J., De la CRUZ, R. & GUIVEL, C. 2005. Petrogenesis of the Eocene and Mio-Pliocene alkaline basaltic magmatism in Meseta Chile Chico, southern Patagonia, Chile: evidence for the participation of two slab windows. *Lithos* **82**, 315–43.

FITZGERALD, M. G., MITCHUM, R. M., ULIANA, M. A. & BIDDLE, K. T. 1990. Evolution of the San Jorge Basin, Argentina. *American Association of Petroleum Geologists Bulletin* **74**, 879–920.

FOLEY, S. F., VENTURELLI, G., GREEN, D. H. & TOSCANI, L. 1987. The ultrapotassic rocks: characteristics, classification, and constraints for petrogenetic models. *Earth Science Reviews* **24**, 81–134.

FUTA, K. & STERN, C. R. 1988. Sr and Nd isotopic and trace element composition of Quaternary volcanic centers of southern Andes. *Earth and Planetary Science Letters* **88**, 253–63.

GERLACH, D. C., FREY, F. A., MORENO-ROA, H. & LÓPEZ-ESCOBAR, L. 1988. Recent volcanism in the Puyehue–Cordon Caulle region, Southern Andes, Chile (40.5°S): petrogenesis of evolved lavas. *Journal of Petrology* **29**, 333–82.

GORRING, M. L. & KAY, S. M. 2000. Carbonatite metasomatized peridotite xenoliths from southern Patagonia: implications for lithospheric processes and Neogene plateau magmatism. *Contributions to Mineralogy and Petrology* **140**, 55–72.

GORRING, M. L. & KAY, S. M. 2001. Mantle processes and sources of Neogene slab window magmas from southern Patagonia, Argentina. *Journal of Petrology* **42**, 1067–94.

GORRING, M. L., KAY, S. M., ZEITLER, P. K., RAMOS, V. A., RUBIOLO, D., FERNANDEZ, M. I. & PANZA, J. L. 1997. Neogene Patagonian plateau lavas: Continental magmas associated with ridge collision at the Chile Triple Junction. *Tectonics* **16**, 1–17.

GORRING, M. L., SINGER, B., GOWERS, J. & KAY, S. M. 2003. Plio-Pleistocene basalts from the Meseta del Lago Buenos Aires, Argentina: evidence for asthenosphere–

lithosphere interactions during slab window magmatism. *Chemical Geology* **193**, 215–35.

GRIPP, A. E. & GORDON, R. G. 2002. Young tracks of hotspots and current plate velocities. *Geophysical Journal International* **150**, 321–61.

GUIVEL, C., MORATA, D., PELLETER, E., ESPINOZA, F., MAURY, R. C., LAGABRIELLE, Y., POLVÉ, M., BELLON, H., COTTEN, J., BENOIT, M., SUÁREZ, M. & DE LA CRUZ, R. 2006. Miocene to Late Quaternary Patagonian basalts (46–47°S): geochronometric and geochemical evidence for slab tearing due to active spreading ridge subduction. *Journal of Volcanology and Geothermal Research* **149**, 346–70.

HART, S. R. 1984. The DUPAL anomaly: a large-scale isotopic anomaly in the southern hemisphere. *Nature* **309**, 753–6.

HART, S. R., HAURI, E. H., OSCHMANN, L. A. & WHITEHEAD, J. A. 1992. Mantle plumes and entrainment: isotopic evidence. *Science* **256**, 517–20.

HECHEM, J. J. & STRELKOV, E. 2002. Secuencia sedimentaria mesozoica del Golfo San Jorge. In *Geología y Recursos Naturales de Santa Cruz* (ed. M. J. Haller), pp. 129–47. Relatorio del XV Congreso Geológico Argentino, Buenos Aires, Argentina.

HERVÉ, F., DAVIDSON, J., MPODOZIS, E. & COVACEVICH, E. V. 1981. The late Palaezoic in Chile: stratigraphy, structure and possible tectonic framework. *Anais da Academia Brasileira de Ciências* **53**, 361–73.

HICKEY, R., FREY, F. A. & GERLACH, D. 1986. Multiple sources for basaltic arc rocks from the Southern Volcanic Zone of the Andes (34°–41°S): trace element and isotopic evidence for contributions from subducted oceanic crust, mantle, and continental crust. *Journal of Geophysical Research* **91**, 5963–83.

HICKEY-VARGAS, R., MORENO-ROA, H., LÓPEZ-ESCOBAR, L. & FREY, F. A. 1989. Geochemical variations in Andean basaltic and silicic lavas from the Villarrica–Lanin volcanic chain (39.5° S): an evaluation of source heterogeneity, fractional crystallization and crustal assimilation. *Contributions to Mineralogy and Petrology* **103**, 361–86.

HIROSE, K. & KUSHIRO, I. 1993. Partial melting of dry peridotite at high pressures: determination of compositions of melts segregated from peridotite using aggregates of diamond. *Earth and Planetary Science Letters* **114**, 477–89.

HOLE, M. J., KEMPTON, P. D. & MILLAR, I. L. 1993. Trace-element and isotopic characteristics of small-degree melts of the asthenosphere: evidence from the alkalic basalts of the Antarctic Peninsula. *Chemical Geology* **109**, 51–68.

HOLE, M. J., SAUNDERS, A. D., ROGERS, G. & SYKES, M. A. 1995. The relationship between alkaline magmatism, lithospheric extension and slab window formation along continental destructive plate margins. In *Volcanism associated with extension at consuming plate margins* (ed. J. L. Smellie), pp. 265–85. Geological Society of London, Special Publication no. 81.

HOMOVC, J. F., CONFORTO, G. A., LAFOURCADE, P. A. & CHELOTTI, L. A. 1995. Fold beld in the San Jorge Basin, Argentina: an example of tectonic inversion. In *Basin Inversion* (eds J. G. Buchanan & P. G. Buchanan), pp. 235–48. Geological Society of London, Special Publication no. 88.

KAY, S. M., ARDOLINO, A. A., GORRING, M. L. & RAMOS, V. A. 2007. The Somuncura large igneous province in Patagonia: interaction of a transient mantle thermal anomaly with a subducting slab. *Journal of Petrology* **48**, 43–77.

KAY, S. M. & COPELAND, P. 2006. Early to middle Miocene backarc magmas of the Neuquén Basin: Geochemical consequences of slab shallowing and the westward drift of South America. In *Evolution of an Andean margin: a tectonic and magmatic view from the Andes to the Neuquén Basin (35°–39° S lat)* (eds S. M. Kay & V. A. Ramos), pp. 185–213. Geological Society of America, Special Paper no. 407.

KEMPTON, P. D., HAWKESWORTH, C. J., LOPEZ-ESCOBAR, L., PEARSON, D. G. & WARE, A. J. 1999. Spinel ± garnet lherzolite xenoliths from Pali Aike: Part 2, Trace element and isotopic evidence bearing on the evolution of lithospheric mantle beneath southern Patagonia. In *The J. B. Dawson volume* (eds J. J. Gurney, J. L. Gurney, M. D. Pascoe & S. H. Richardson), pp. 415–28. Proceedings of the 7th International Kimberlite Conference, Red Rood Design, Cape Town, South Africa.

KLEMME, S. & O'NEILL, H. ST. C. 2000. The near-solidus transition from garnet lherzolite to spinel lherzolite. *Contributions to Mineralogy and Petrology* **138**, 237–48.

KOGISO, T., TATSUMI, Y. & NAKANO, S. 1997. Trace element transport during dehydration processes in the subducted oceanic crust: 1. Experiments and implications for the origin of ocean island basalts. *Earth and Planetary Science Letters* **148**, 193–205.

KUSHIRO, I. 2001. Partial melting experiments on peridotite and origin of mid-ocean ridge basalt. *Annual Review of Earth and Planetary Science* **29**, 71–107.

LIZUAIN, A., RAGONA, D. & FOLGUERA, A. 1995. *Mapa Geológico de la Provincia del Chubut, República Argentina. Secretaría de Minería, Dirección Nacional del Servicio Geológico, Scale 1:750.000*. Buenos Aires, Argentina.

LÓPEZ-ESCOBAR, L., KILIAN, R., KEMPTON, P. & TAGIRI, M. 1993. Petrography and geochemistry of Quaternary rocks from the Southern Volcanic Zone of the Andes between 41°30′ and 46°00′S, Chile. *Revista Geológica de Chile* **20**, 33–55.

LÓPEZ-ESCOBAR, L., PARADA, M. A., HICKEY-VARGAS, R., FREY, F. A., KEMPTON, P. D. & MORENO, H. 1995. Calbuco Volcano and minor eruptive centers distributed along the Liquiñe–Ofqui Fault Zone, Chile (41°–42° S): contrasting origin of andesitic and basaltic magma in the Southern Volcanic Zone of the Andes. *Contribution to Mineralogy and Petrology* **119**, 345–61.

MARSHALL, L. G., CIFELLI, R. L., DRAKE, R. E. & CURTIS, G. H. 1986. Vertebrate paleontology, geology and geochronology of the Tapera de López and Scarritt Pocket, Chubut Province, Argentina. *Journal of Paleontology* **60**, 920–51.

MASSAFERRO, G. I., HALLER, M. J., D'ORAZIO, M. & ALRIC, V. I. 2006. Sub-recent volcanism in Northern Patagonia: a tectonomagmatic approach. *Journal of Volcanology and Geothermal Research* **155**, 227–43.

MCDONOUGH, W. F. & SUN, S. S. 1995. The composition of the Earth. *Chemical Geology* **120**, 223–53.

NTAFLOS, TH., BJERG, E. A., LABUDIA, C. H. & KURAT, G. 2007. Depleted lithosphere from the mantle wedge beneath Tres Lagos, southern Patagonia, Argentina. *Lithos* **94**, 46–65.

PANKHURST, R. J. & RAPELA, C. R. 1995. Production of Jurassic rhyolite by anatexis of the lower crust of Patagonia. *Earth and Planetary Science Letters* **134**, 23–36.

PANKHURST, R. J., RAPELA, C. W., FANNING, C. M. & MÁRQUEZ, M. 2006. Gondwanide continental collision and origin of Patagonia. *Earth Science Reviews* **76**, 235–56.

PEARCE, T. H. 1978. Olivine fractionation equations for basaltic and ultrabasic liquids. *Nature* **276**, 771–4.

PLÁ CID, J., NARDI, L. V. S., GISBERT, P. E., MERLET, C. & BOYER, B. 2005. SIMS analyses on trace and rare earth elements in coexisting clinopyroxene and mica from minette mafic enclaves. *Contributions to Mineralogy and Petrology* **148**, 675–88.

QUARTINO, B. J. 1958. El basalto olivínico del Cerro El Pedrero, Chubut. *Revista de la Asociación Geológica Argentina* **12**, 233–64.

RAMOS, V. A. & KAY, S. M. 1992. Southern Patagonian plateau basalts and deformation: backarc testimony of ridge collisions. *Tectonophysics* **205**, 261–82.

RIVALENTI, G., MAZZUCCHELLI, M., LAURORA, A., CIUFFI, S. I. A., ZANETTI, A., VANNUCCI, R. & CINGOLANI, C. A. 2004. The backarc mantle lithosphere in Patagonia, South America. *Journal of South American Earth Sciences* **17**, 121–52.

RIVALENTI, G., MAZZUCCHELLI, M., ZANETTI, A., VANNUCCI, R., BOLLINGER, C., HÉMOND, C. & BERTOTTO, G. W. 2007. Xenoliths from Cerro de los Chenques (Patagonia): An example of slab-related metasomatism in the backarc lithospheric mantle. *Lithos* **99**, 45–67.

SCHILLING, M., CONCEIÇÃO, R. V., MALLMANN, G., KOESTER, E., KAWASHITA, K., HERVÉ, F., MORATA, D. & MOTOKI, A. 2005. Spinel-facies mantle xenoliths from Cerro Redondo, Argentine Patagonia: petrographic, geochemical, and isotopic evidence of interaction between xenoliths and host basalt. *Lithos* **82**, 485–502.

SCOPPOLA, B., BOCCALETTI, D., BEVIS, M., CARMINATI, E. & DOGLIONI, C. 2006. The westward drift of the lithosphere; a rotational drag? *Geological Society of America Bulletin* **118**, 199–209.

SHERVAIS, J. W. 1982. Ti–V plots and the petrogenesis of modern and ophiolitic lavas. *Earth and Planetary Science Letters* **59**, 101–18.

SPERA, F. J. & BOHRSON, W. A. 2001. Energy-constrained open-system magma processes I: general model and energy-constrained assimilation fractional-crystallization (EC-AFC) formulation. *Journal of Petrology* **42**, 999–1018.

STEIGER, K. H. & JÄGER, E. 1977. Subcommission on geochronology: Convention on the use of decay constants in geo- and cosmochronology. *Earth and Planetary Science Letters* **36**, 359–62.

STERN, C. R., FREY, F. A., FUTA, K., ZARTMAN, R. E., PENG, Z. & KYSER, T. K. 1990. Trace-element and Sr, Nd, Pb and O isotopic composition of Pliocene and Quaternary alkali basalt of the Patagonian Plateau lavas of southernmost South America. *Contributions to Mineralogy and Petrology* **104**, 294–308.

STERN, C. R. & KILIAN, R. 1996. Role of the subducted slab, mantle wedge and continental crust in the generation of adakites from the Andean Austral Volcanic Zone. *Contributions to Mineralogy and Petrology* **123**, 263–81.

STERN, C. R., KILIAN, R., OLKER, B., HAURI, E. H. & KYSER, T. K. 1999. Evidence from mantle xenoliths for relatively thin (< 100 km) continental lithosphere below the Phanerozoic crust of southernmost South America. *Lithos* **48**, 217–35.

STURM, M. E., KLEIN, E. M., GRAHAM, D. W. & KARSTEN, J. 1999. Age constraints on crustal recycling to the mantle beneath the southern Chile Ridge: He–Pb–Sr–Nd isotope systematics. *Journal of Geophysical Research* **104**, B3, 5097–114.

SUDO, A. & TATSUMI, Y. 1990. Phlogopite and K-amphibole in the upper mantle: implication for magma genesis in subduction zones. *Geophysical Research Letters* **17**, 29–32.

SUN, S. S. & MCDONOUGH, W. F. 1989. Chemical and isotopic systematics of oceanic basalts: implications for mantle composition and processes. In *Magmatism in the Ocean Basins* (eds A. D. Saunders & M. J. Norry), pp. 313–45. Geological Society of London, Special Publication no. 42.

SYLWAN, C. A. 2001. Geology of the Golfo San Jorge Basin, Argentina. *Journal of Iberian Geology* **27**, 123–57.

TAYLOR, S. R. & MCLENNAN, S. M. 1995. The geochemical evolution of the continental crust. *Reviews in Geophysics* **33**, 241–65.

THYBO, H. 2006. The heterogeneous upper mantle low velocity zone. *Tectonophysics* **416**, 53–79.

TIEPOLO, M., ZANETTI, A., OBERTI, R., BRUMM, R., FOLEY, S. & VANNUCCI, R. 2003. Trace-element partitioning between synthetic potassic richterites and silicate melts, and contrasts with the partitioning behaviour of pargasites and kaersutites. *European Journal of Mineralogy* **15**, 329–40.

TODT, W., CLIFF, R. A., HANSER, A. & HOFMANN, A. W. 1996. Evaluation of a ^{202}Pb–^{205}Pb double spike for high-precision lead isotope analysis. In *Earth processes: reading the isotopic code* (eds S. R. Hart & A. Basu), pp. 429–37. American Geophysical Union, Geophysical Monograph vol. 95. Washington, DC, USA.

VERNIERES, J., GODARD, M. & BODINIER, J.-L. 1997. A plate model for the simulation of trace element fractionation during partial melting and magmas transport in the Earth's upper mantle. *Journal of Geophysical Research* **102**, 24771–84.

WAGNER, T. P. & GROVE, T. L. 1998. Melt/harzburgite reaction in the petrogenesis of tholeiitic magma from Kilauea volcano, Hawaii. *Contributions to Mineralogy and Petrology* **131**, 1–12.

XU, Y. G., MA, J. L., FREY, F. A., FEIGENSON, M. D. & LIU, J. F. 2005. Role of lithosphere–asthenosphere interaction in the genesis of Quaternary alkali and tholeiitic basalts from Datong, western North China Craton. *Chemical Geology* **224**, 247–71.

Appendix. Analytical methods

Major and trace element analyses were performed at Pisa University's Dipartimento di Scienze della Terra. Major elements were determined by X-ray fluorescence on an ARL 9400 XP+ spectrometer using $Li_2B_4O_7$ glass disks (sample:flux ratio = 1:7). Estimated precision (relative standard deviation, RSD) is about 1 % for SiO_2 and about 2 % for the other major elements except those with low concentrations ($\sim$ < 0.50 wt %), for which the absolute standard deviation is about $\pm$ 0.01 %. Loss on ignition (LOI) was determined by gravimetry at 1000 °C after pre-heating at 110 °C.

The concentrations of a set of thirty-five trace elements were determined by inductively coupled plasma–mass spectrometry (VG PQII Plus). Sample powders were dissolved in PFA vessels on a hot plate at about 120 °C using HF + HNO_3. The sample solutions, spiked with Rh, Re and Bi as internal standards, were measured by external calibration using international reference materials of basaltic composition. Analytical precision, assessed by repeated

analysis of the in-house standard HE-1 (Mt Etna hawaiite), is between 2 and 5 % RSD, except for Gd, Tm, Be, Sc, Pb (6–8 % RSD).

Sr, Nd and Pb isotope compositions were measured with a Finnigan MAT 262V multicollector mass spectrometer at the CNR Istituto di Geoscienze e Georisorse in Pisa. Conventional ion exchange methods were used for Sr, Nd and Pb separations. Measured $^{87}Sr/^{86}Sr$ ratios were normalized to $^{86}Sr/^{88}Sr = 0.1194$; $^{143}Nd/^{144}Nd$ ratios were normalized to $^{146}Nd/^{144}Nd = 0.7219$. During the collection of isotopic data for this study, replicate measurements of NIST SRM 987 ($SrCO_3$) and La Jolla standards yielded values of 0.710243 $\pm$ 13 (2σ, N = 20) for $^{87}Sr/^{86}Sr$ and 0.511848 $\pm$ 7 (2σ, N = 30) for $^{143}Nd/^{144}Nd$. Lead was loaded on Re filaments with tetraethyl orthosilicate as activator. Replicate analyses (N = 50) of NIST SRM 981 (natural lead) indicate that Pb isotope ratios are measured with a precision of 0.03 % (2σ) per mass unit. Mass fractionation was corrected for by applying a factor of 0.14 $\pm$ 0.01 % per mass unit (NIST SRM 981 certified values after Todt *et al.* 1996).

Potassium/argon analyses were carried out at the Institute of Nuclear Research of the Hungarian Academy of Sciences. The groundmass of fourteen samples was separated through standard separation techniques and purified by hand-picking under a stereo-microscope. Groundmass samples, which show intersertal or intergranular texture and are fresh or very weakly altered, have been chosen for the analytical work because the xenocrysts/xenoliths occurring in some basalts can strongly affect the radiometric age. About 500 mg of sample were spiked with ^{38}Ar for the determination of ^{40}Ar. The mass spectrometer, operating in static mode, was cleaned with conventional getter material prior to gas sample introduction. The HD-B1, GL-O, LP-6 and Asia 1/65 interlaboratory standards were used for calibration. Ages were calculated using the decay constants of Steiger & Jäger (1977). All analytical errors represent one standard deviation. Potassium concentrations were determined by flame photometry, and replicate analyses were reproducible within 2 %. Further details are reported in Balogh (1985).